Supplemental Material: Annu. Rev. Biochem. 2011. 80:669-702
doi: 10.1146/annurev-biochem-060409-092741

Biological Phosphoryl Transfer Reactions:
Understanding Mechanism and Catalysis
Lassila, Zalatan, Herschlag

Contents:

A. Rate Constants for Nonenzymatic Attack by Water

Measured or estimated nonenzymatic rate constants for attack by neutral water at 25 °C on compounds with the 4-nitrophenolate leaving group are reported here.

Table A1. Nonenzymatic rate constants for water attack at 25 °C.

Structure	Compound	Rate constant, M^{-1} s^{-1}	Source
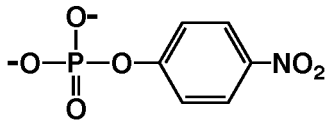	$pNPP^{2-}$	3.0×10^{-11}	Calculated from published rate constant at 39 °C and temperature dependence (1). Second-order rate constant obtained by dividing by the concentration of water, 55.5 M.
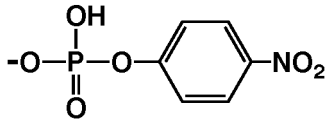	$pNPP^{-}$	3.0×10^{-9}	Calculated from published rate constant at 39 °C and temperature dependence of the reaction of 2,4-dinitrophenyl phosphate monoanion (2). Second-order rate constant obtained by dividing by the concentration of water, 55.5 M.
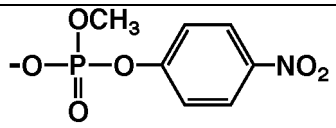	$MepNPP^{-}$	3.3×10^{-12}	Measured 2nd order rate constant with hydroxide at 25 °C was corrected for nucleophile strength (3).
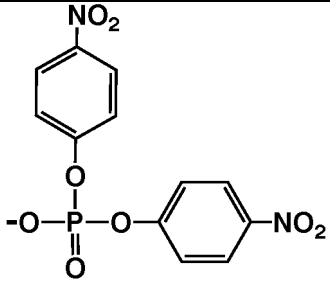	Bis-$pNPP^{-}$	2.9×10^{-13}	Value at 100°C was corrected to 25°C using published temperature dependence (4, 5).
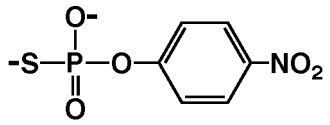	$pNPPS^{2-}$	2.0×10^{-10}	Rate constant corrected to 25 °C using the published temperature dependence (6).
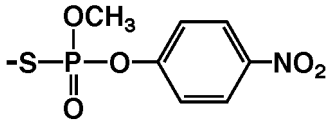	$MepNPPS^{-}$	9.4×10^{-13}	Values within 3-fold were obtained from two methods and averaged: 2nd order rate constant for hydroxide attack at 25 °C corrected for nucleophile strength gives 1.4×10^{-12} (3); value for MepNPP corrected for 7-fold thio-effect gives 4.7×10^{-13} (3, 7).
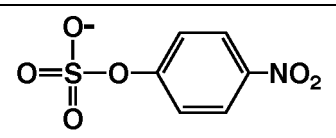	$pNPS^{-}$	9.0×10^{-12}	Published rate constant corrected to 25 °C using published temperature dependence (8, 9). Similar to measured pH-independent rate constant at 30 °C (10).

B. Cases With Evidence for Stepwise Reactions

In a few specific cases, evidence exists for stepwise, rather than concerted, phosphoryl transfer reactions. These specific cases are instructive, and they support the picture from the concerted reactions of loose transition states for monoesters with increasing tightness for diesters and triesters.

Monoesters

For some phosphoryl transfers to alcohol acceptors in organic solvents, racemization of stereochemistry is observed, suggesting the presence of a freely diffusing metaphosphate intermediate (11-14). These reactions in organic solvents involved either hindered nucleophiles (11, 12) or extremely labile leaving groups (13, 14), which may alter the energy landscape in favor of metaphosphate. As discussed in the main text (in the section on Other Tools), and in Section E of this Supplement, racemization of stereochemistry has also been observed in reactions of phosphorothioates, suggestive of free thiometaphosphate (15, 16). These observations can be understood in the context of the two-dimensional reaction coordinate diagram as perturbations that destabilize the upper left (phosphorane) corner and stabilize the lower right (metaphosphate) corner of reactions that proceed through loose transition states, resulting in a local energetic minimum along the reaction pathway in the lower right (metaphosphate) corner.

A metaphosphate intermediate has also been suggested in the hydrolysis reaction of μ-monothiopyrophosphate, an analog of pyrophosphate in which the bridging oxygen atom is replaced by sulfur (17, 18). For this compound, high concentrations of nucleophiles do not increase the reaction rate, but these nucleophiles do capture the phosphoryl group in competition with water, consistent with a discrete, highly-reactive metaphosphate intermediate that is indiscriminately captured by solvating phosphoacceptors (18). This type of reaction, in which a discrete intermediate forms but its lifetime is too short to freely diffuse, is referred to as a preassociation reaction (19). Again, this observation can be understood in the context of a two-dimensional reaction coordinate diagram in which the P-S bond, which is much weaker than a P-O bond and therefore easier to break (18), destabilizes the upper left (phosphorane) and lower left (reactant) corners, possibly leading to a local energetic minimum in the lower right (metaphosphate) corner.

We are not aware of any evidence for phosphorane intermediates in reactions of monoesters (see also Section H of this Supplement).

Diesters

In contrast to the case for monoesters, we are not aware of any evidence for substituted metaphosphate intermediates in diester and triester reactions. However, under specific conditions, some reactions proceed in a stepwise manner through stable phosphorane intermediates. Under acidic and buffer-catalyzed conditions, kinetic evidence supports formation of cyclic pentacoordinate intermediates in ribonucleotides by attack of the 2'-hydroxyl (20-24). In these cases, protonation of the phosphoryl oxygen atoms and the formation of a 5-membered ring may serve to render the diester triester-like and stabilize the phosphorane species sufficiently to allow a stable intermediate. Isotope effect studies have also suggested that some

reactions of diesters associated with Co(III) complexes may proceed through phosphorane intermediates (25). Co(III)-ligand interactions are very stable (26, 27), and therefore addition of Co(III) may mimic addition of covalent substituents in a cyclic structure, providing stabilization to the phosphorane species.

Triesters

Reactions of cyclic phosphotriesters show evidence of stepwise reaction pathways through phosphorane intermediates under certain conditions (28-30). As with diesters, the cyclic structure may play a role in stabilizing the phosphorane intermediate. When β_{LG} was plotted as a function of pK_a of the nucleophile for a set of reactions (a p_{xy} plot, as discussed in Section C), a break in linearity was observed, consistent with a change from concerted to stepwise mechanisms as the nucleophile becomes more basic (29). As discussed further in Section C, increasing the pK_a of the nucleophile can be understood in the context of the two-dimensional reaction coordinate diagram as an effect that destabilizes the free nucleophile, raising the energy of the reactant state and the metaphosphate states, resulting in Hammond and anti-Hammond effects, respectively. The result of these perturbations is an expected move of the transition state horizontally toward the phosphorane intermediate corner. A change from concerted reactions to stepwise phosphorane mechanisms with increasing nucleophile pK_a is therefore consistent with the expected direction of stabilization from two-dimensional reaction coordinate diagrams.

C. Linear Free Energy Relationships: Supplemental Discussion

Effective charge

In addition to the Leffler α parameter, which is used here and in the main text to relate β_{NUC} and β_{LG} to charge development in the transition state, another way to interpret β values is in terms of effective charge. The concept of effective charge uses the pK_a scale as a basis from which to calculate changes in charge on specific atoms by defining the deprotonation equilibrium as a change in charge from neutral to -1. These values are not equivalent to partial charges on the atoms. Instead, the effective charge is an empirical parameter that represents the sensitivity of a reaction to substituent effects, relative to substituent effects on deprotonation (31, 32).

The reaction of phenyl phosphate introduced in the main text is used as an example here (Figure C1). In this example, the oxygen atom of the phenolate product is defined as having a -1 charge and the neutral phenol as having 0 charge (31, 32). Because the phenolate reaction product has been defined to have charge -1 and the value of β_{EQ} = -1.35 (33) implies a change in effective charge of -1.35 units in going from reactants to products, the oxygen in the phenyl phosphate reactant has an effective charge of +0.35 (Figure C1). Thus, the oxygen behaves as if the phosphoryl group is more electron withdrawing than a proton. Applying this same logic, by adding the β_{LG} value of -1.26 to the reactant charge of +0.35, we obtain an effective charge of -0.91 in the phenolate oxygen in the transition state. This value suggests that in the transition state for phosphate monoester hydrolysis, the leaving group oxygen has nearly the full charge of the product.

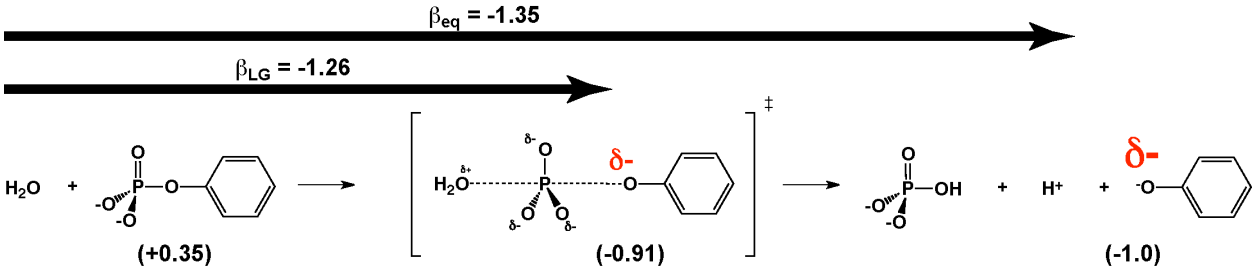

Figure C1. Example of the use of effective charge. If we define the charge on the phenolate oxygen as -1, the β_{EQ} value of -1.35 (33) implies that the same oxygen has an effective charge of +0.35 in the phenyl phosphate reactant. The β_{LG} value of -1.26 gives an effective charge of -0.91 for the oxygen in the transition state.

Experimental Results for Monoesters, Diesters, and Triesters

Results from roughly 90 individual LFER experiments for monoesters, diesters, and triesters are tabulated in Section D. Here, we will describe lessons arising from this large data set and, remarkably, limitations that remain despite this wealth of data.

The data from these LFERs are plotted in Figure C2 in terms of α, which reflects an estimate for the extent of bonding in the transition state, as described in the main text. The red and blue points reflect data from β_{LG} and β_{NUC} experiments, respectively.

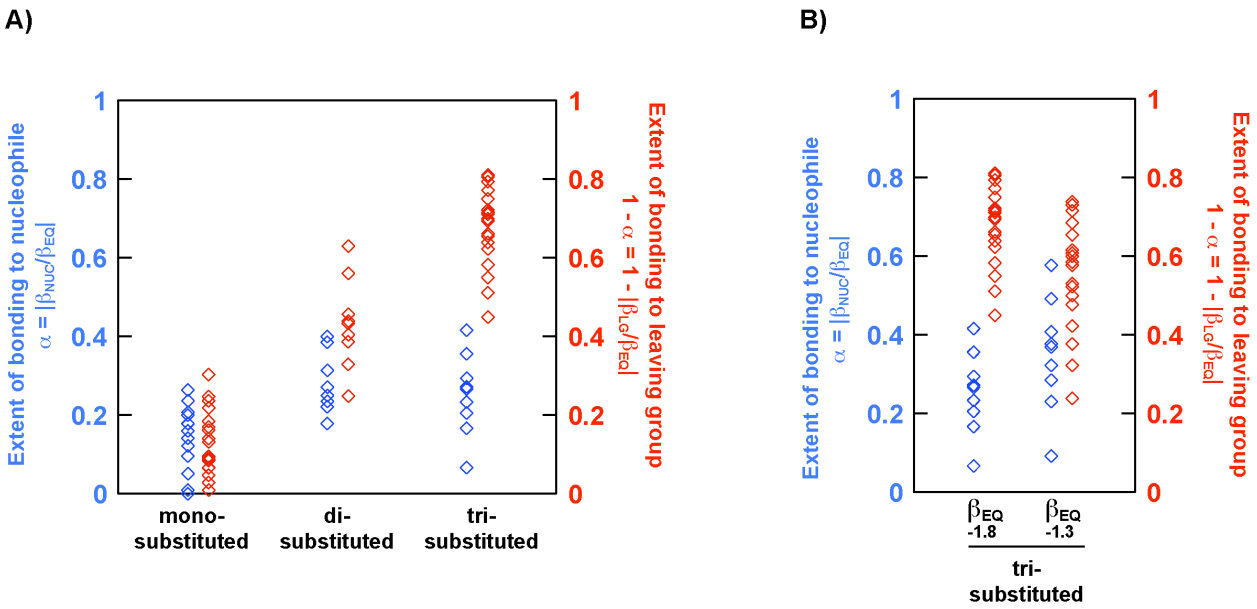

Figure C2. LFER results from the literature. **(A)** Data from Section D are plotted for monosubstituted, disubstituted, and trisubstituted compounds. Values of β_{NUC} (blue) and β_{LG} (red) are plotted in terms of α to reflect bonding in the transition state. Values of β_{EQ} used in (A) for oxygen nucleophiles and leaving groups were from Bourne and Williams (33): monosubstituted compounds, β_{EQ} = -1.35, disubstituted compounds, β_{EQ} = -1.73, trisubstituted compounds, -1.82. For nitrogen nucleophiles and leaving groups, the following values were used: monosubstituted compounds, -1.05 (34); disubstituted compounds -1.4 (See Table D15). Four data points with $\beta_{NUC} < 0$ apparently arising from desolvation effects (35) are not shown in the plot for clarity, and no correction for amine desolvation was made for the data shown (35). Including this correction does not change the appearance or interpretation of the plot. **(B)** The value of β_{EQ} used substantially affects the appearance of asymmetry in the plots. The data for triesters are plotted using values of β_{EQ} = -1.8 (33) and β_{EQ} = -1.3 (36), as indicated. The asymmetry is discussed further in this section.

As discussed in the main text, the data for monosubstituted compounds indicate a low apparent fractional bonding for both the nucleophile and leaving group, consistent with loose transition states. In the progression from monosubstituted to trisubstituted compounds, the values increase, suggesting increasingly tight transition states. In addition, an increasing variability of bonding in the transition state is seen with increasing esterification. Figure C2A also suggests an additional trend, an increase in apparent asymmetry in measured values from β_{NUC} and β_{LG} experiments. We discuss this asymmetry in the following paragraphs.

In the text we have generally described concepts about transition states using examples with symmetrical reactions. In a symmetrical reaction with an identical nucleophile and leaving group, the transition state is located along the diagonal between the lower right corner and the upper left corner of Figure 3C in the main text. In such a situation we can estimate the extent of bonding in the transition state from β_{NUC} and β_{LG} values as follows. For phosphoryl transfer from phosphorylated pyridine to pyridine, for example, we take the β_{NUC} value from LFERs for reactions with a pyridine leaving group and a series of nucleophiles with pK_a values above and below those of pyridine. We would also use a value of β_{LG} obtained using a pyridine nucleophile and a series of leaving groups with pK_a values above and below those of pyridine. The value for β_{EQ} would be used to calculate values for α, and these values could be placed on a two-dimensional reaction coordinate diagram. As seen in the data tables in Section D, there are insufficient data to follow this procedure directly for symmetric reactions because many of the necessary series of compounds have not been studied. Nevertheless, consideration of the expectations for symmetric reactions is helpful in analyzing the available data.

As seen in Figure C2A, diesters and triesters show asymmetry in the extent of bonding that is calculated from values of β_{NUC} and β_{LG}. According to the law of microscopic reversibility, symmetric reactions with a single transition state must in principle have the same degree of bonding to the nucleophile and leaving group in the transition state. In other words, because the nucleophile and leaving group are indistinguishable in a symmetric reaction, the values of $|\alpha|$ and $|1- \alpha|$ obtained from β_{NUC} and β_{LG} experiments should be identical. Thus, in a dataset of LFER values in which possible compounds and pK_a values are sampled fully without bias, the ranges of measured values of $|\alpha|$ and $|1- \alpha|$ should be the same and the red and blue points in Figure C2A should align. In contrast to this expectation, Figure C2A shows separation between the red and blue points, and this separation increases in the progression from monoesters to diesters to triesters.

One potential cause of this observed asymmetry is incompleteness of the available data. Some ranges of pK_a values have not been tested in experiments, because many studies use strong nucleophiles (high pK_a) and good leaving groups (low pK_a) to ensure an adequate rate enhancement over the hydrolysis reaction by the added nucleophile and to render the reaction fast enough to conveniently follow. This bias would not be a problem if β_{NUC} values were independent of the leaving group pK_a and vice versa. However, these values are interdependent. The interdependence of these values as well as the gaps in the available data are described below in the discussion of p_{xy} values.

A second possible cause of the observed asymmetry is the choice of β_{EQ} values used to obtain α. As discussed in the main text, values of β_{EQ} are difficult to obtain, particularly for reactions where one side of the equilibrium is strongly favored. We use the data for triesters to illustrate the effect of changing β_{EQ} on the appearance of asymmetry. In Figure C2B, two different estimates of β_{EQ} are used to plot the same set of triester LFER data. The results plotted in terms of α values show substantial differences in the degree of asymmetry. When the value of $\beta_{EQ} = -1.3$ is used, the asymmetry is reduced substantially relative to when $\beta_{EQ} = -1.8$ is used. The value of $\beta_{EQ} = -1.3$ was estimated from individual experiments to measure β_{NUC} and β_{LG}, where

$\beta_{EQ} = (\beta_{LG} - \beta_{NUC})$ (36). This value has the limitation that biases in the type, number, and range of compounds selected for LFERs can impact the resulting β values. The value of $\beta_{EQ} = -1.8$ was estimated by using the protonation of the phosphoryl oxygens as an approximation of adding esterifying substituents for diesters and triesters (33). This value has the limitation that alkyl and aryl substituents could potentially affect β_{EQ} differently than do protons. Further work is needed to obtain more direct estimates of β_{EQ}, to obtain LFER data for wider ranges of compounds and pK_a values, and to understand the potential differential effects of esterifying substitutents.

In summary, while the data for monoesters are relatively complete, considerably more data are required to obtain a full set of values for diesters and triesters that would help define the range of transition state structures. Data for symmetric reactions are particularly needed. Further, one would like to have available corresponding KIE data over this series.

The p_{xy} coefficient

In an experiment in which the leaving group is varied for a series of reactions with a common nucleophile, the slope of the dependence of reactivity on pK_a is referred to as β_{LG}, as described in the main text. But different values of β_{LG} can be obtained with different nucleophiles. The slope of the dependence of β_{LG} on nucleophile pK_a is called a p_{xy} coefficient and is described by the equation below (37). There is symmetry to this relationship, and the same slope, or p_{xy} coefficient, is obtained by determining the dependence of β_{NUC} on the leaving group pK_a. Measured differences in p_{xy} coefficients obtained from β_{NUC} or β_{LG} data arise from differences in the data used and/or experimental and fitting error.

$$p_{xy} = \frac{\partial \beta_{LG}}{\partial pK_{NUC}} = \frac{\partial \beta_{NUC}}{\partial pK_{LG}} = \frac{\partial^2 \log k}{\partial pK_{NUC} \partial pK_{LG}}$$

Although not commonly discussed, the p_{xy} value is highly useful as it can relate observed trends in LFERs to expectations from energetic effects on two-dimensional reaction coordinate diagrams (see below). Related important concepts are p_x and p_y. While p_{xy} applies to changes across multiple LFERs, p_x and p_y refer to changes within a single LFER. In other words, p_x and p_y express the curvature of the LFER itself. In an experiment to measure β_{NUC}, the p_x value is the dependence of β_{NUC} on the nucleophile pK_a. In an experiment to measure β_{LG}, p_y is the dependence of β_{LG} on the leaving group pK_a. These values are more difficult to determine than p_{xy} coefficients because it is harder to detect curvature in a single set of experimental data than it is to detect differing slopes across a series of independent experiments. Nevertheless, large curvatures suggesting substantial changes in β_{NUC} or β_{LG} with pK_a would be evident in many experiments and in practice are not seen. This observation is also consistent with basic predictions from consideration of two-dimensional reaction diagrams (37).

$$p_x = \frac{-\partial \beta_{NUC}}{\partial pK_{NUC}} = \frac{-\partial^2 \log k}{\partial (pK_{NUC})^2} \qquad p_y = \frac{-\partial \beta_{LG}}{\partial pK_{LG}} = \frac{-\partial^2 \log k}{\partial (pK_{LG})^2}$$

In the following set of figures, we present data from Section D for monoesters, diesters and triesters plotted against pK_a to obtain values for the p_{xy} coefficient. These plots show an

increased variability of triester transition states relative to those of monoesters, as discussed above. The plots also illustrate that the available LFER data do not represent complete sampling of the full range of possible pK_a values.

Monoester data are plotted in Figure C3 and fit to a common slope of p_{xy} = 0.017. This value is similar to reported p_{xy} values for monoesters of 0.014 (34) and 0.013 (38). The observation of a small but non-zero p_{xy} value for monoesters provided one of the key pieces of evidence that helped to resolve the question of whether these reactions followed a concerted or stepwise mechanism. The dependence of the bond to the leaving group (β_{LG}) on the identity of the nucleophile means that both are present in the transition state (38).

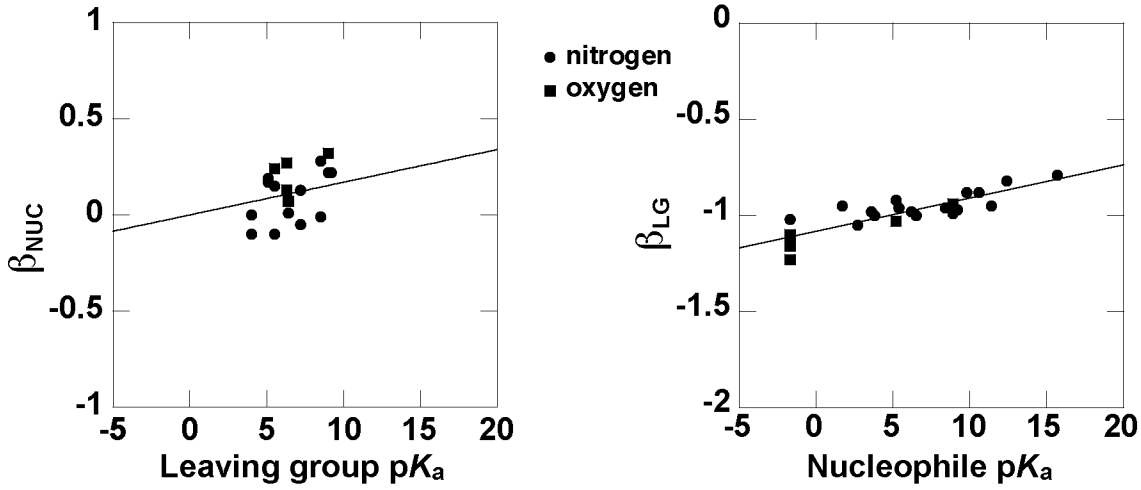

Figure C3. Plots of β vs. pK_a (p_{xy} plots) for monosubstituted compounds. On the left, β_{NUC} values are plotted as a function of the pK_a of the leaving group used in the experiment. Experiments in which series of nitrogen nucleophiles were used are shown with circles, and oxygen nucleophiles in squares. Note that the few slightly negative β_{NUC} values for nitrogen nucleophiles (circles) are likely underestimates of the extent of bonding due to desolvation effects (35). On the right, β_{LG} values are plotted as a function of nucleophile pK_a for series of nitrogen and oxygen leaving groups. Both plots are shown with lines with the same slope of p_{xy} = 0.017, which was the best-fit line for the plot on the right.

Only limited data are available for diesters, and the results are more variable (Figure C4). No attempt was made to fit these values to a line.

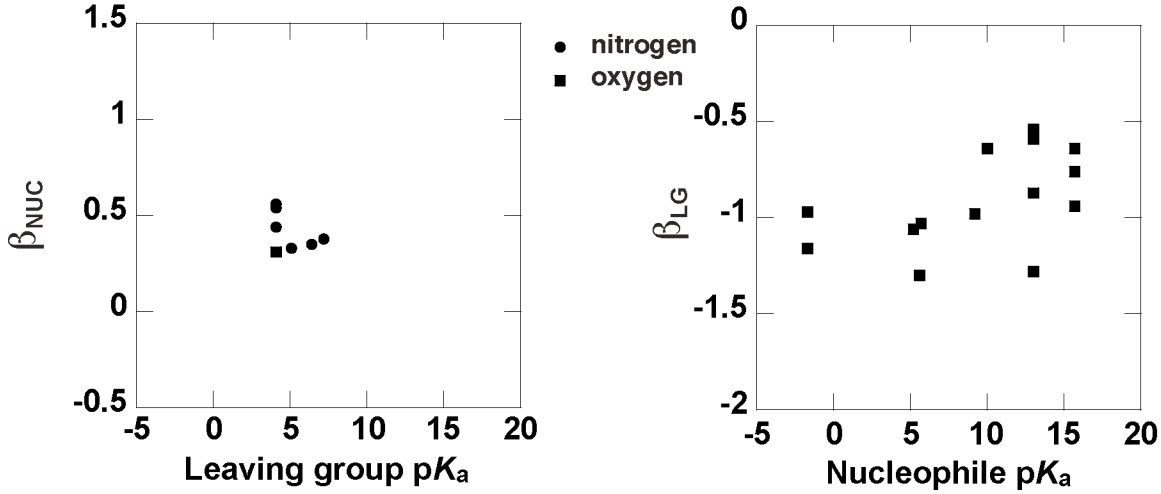

Figure C4. Plots of β vs. pK_a (p_{xy} plots) for disubstituted compounds. On the left, β_{NUC} values are plotted as a function of the pK_a of the leaving group used in the experiment for series of nitrogen and oxygen nucleophiles as indicated. On the right, β_{LG} values are plotted as a function of nucleophile pK_a.

The data for triesters are shown in Figure C5 with a common trend line of slope 0.05. This value is somewhat smaller than a previously reported p_{xy} value of 0.115 (36) but is still substantially steeper than that for phosphate monoesters (see above), as is evident when data for both compounds are plotted together in Figure C6.

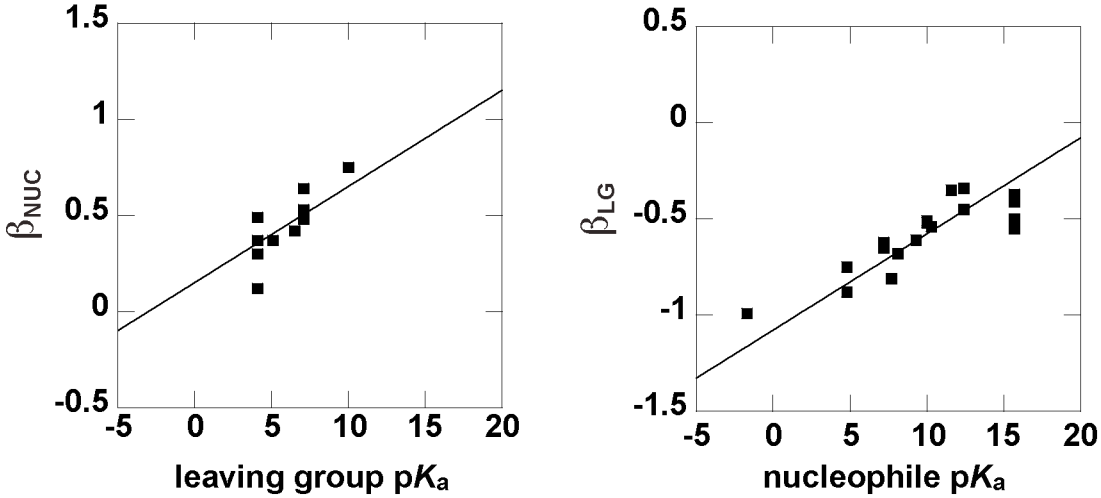

Figure C5. Plots of β vs. pK_a (p_{xy} plots) for phosphate triesters. On the left, β_{NUC} values are plotted as a function of the pK_a of the leaving group. On the right, β_{LG} values are plotted as a function of nucleophile pK_a. Both plots were fit to lines with slope $p_{xy} = 0.05$.

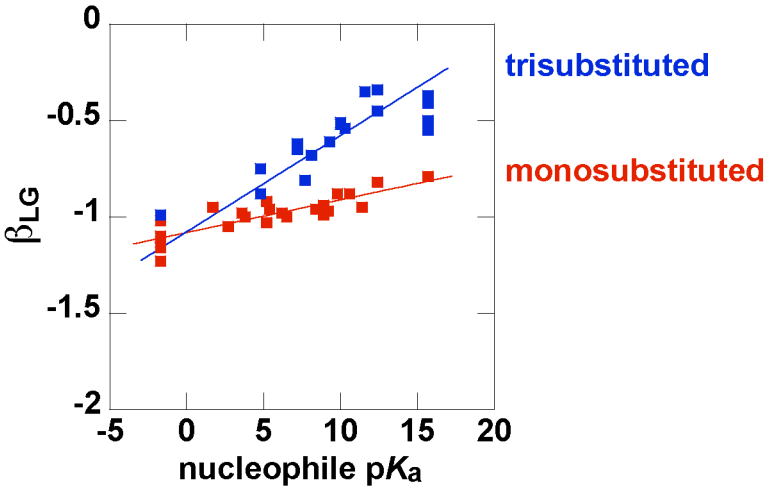

Figure C6. Overlay of p_{xy} plots for monosubstituted and trisubstituted compounds.

Figure C6 illustrates that the measured values for triesters show a steeper dependence on pK_a than do the values for monoesters. This greater dependence on pK_a is reflected in the wider range of observed transition state parameters as illustrated in Figure C2.

Understanding p_{xy} in the context of the two-dimensional reaction coordinate diagram

As discussed above and in the main text, the Leffler α parameter allows us to consider LFER results in the context of a two-dimensional reaction coordinate diagram. This diagram can also be used to understand and model changes related to the p_{xy} coefficient. As described in the main text and below, we can predict the direction of change in transition states based on Hammond and anti-Hammond effects. The example we gave in the main text, in which the phosphorane intermediate was stabilized by the addition of esterifying groups, was the simplest case, as we needed to only consider anti-Hammond effects. There the stabilization of the phosphorane from esterification predicted a movement of the transition state toward the upper left (toward the phosphorane) in going from monoester to diester to triester, consistent with LFER and KIE data.

We now discuss the direction of change of the transition state predicted upon variation of nucleophile or leaving group pK_a, as is measured by the p_{xy} coefficient. The p_{xy}, p_x, and p_y coefficients give us empirical measures changes in transition state structure as a function of pK_a, but we can also predict the direction of change from energetic arguments using the two-dimensional reaction coordinate diagram. In Figure C7A, the blue point represents a loose transition state for the reaction of a phosphate monoester. We consider the effect of increasing the pK_a of the leaving group on this transition state. Increasing the pK_a of the leaving group is equivalent to destabilizing the unbonded leaving group. As this unbonded species is present in the products (upper right corner) and in the hypothetical metaphosphate species (lower right corner), these corners and thus the right side of the energy landscape are increased in energy.

To evaluate the resulting effects on the transition state, we need to consider both Hammond and anti-Hammond effects. The effect of increasing the pK_a of the leaving group on the transition

state can be understood in terms of two vectors, parallel and perpendicular to the reaction pathway. Along the vector parallel to the reaction pathway, the transition state represents a maximum in energy. Changes in this direction give Hammond effects (Figure C7B) (39, 40). The effect of raising the energy of the products in the upper right corner is to move the transition state toward the destabilized species, or toward the upper right corner, as indicated by a red arrow. Along the vector perpendicular to the reaction pathway, the transition state is a minimum in energy. Anti-Hammond effects occur in this direction (Figure C7C), and the result of increasing the energy of the metaphosphate species in the lower right corner is to move the transition state away from the lower right corner, as indicated by the red arrow. Combining these two vectors gives the predicted change in the transition state position, shown with the black arrow.

The transition state moves 'up' on the reaction profile, with increased bonding to the nucleophile (increased β_{NUC}) and no change in the bonding to the leaving group (unchanged β_{LG}). Note that this predicted direction of change assumes that the curvature of the energy surface is similar along both vectors, so that the magnitudes of the predicted effects in each direction are similar. The predictions indeed match what is observed in experimental LFER data. As shown in Figures C3 through C6, as the pK_a of the leaving group is changed, the β_{NUC} value is increased. Similarly, as the pK_a of the nucleophile is increased, the β_{LG} value is increased. The p_{xy} coefficent provides an empirical measure of the magnitude of these changes that reflects the sensitivity of the transition state to changes in the overall energy surface.

Works by Jencks provide more extensive illustration and analysis of the use of two-dimensional reaction coordinate diagrams to predict changes in transition state structure (37, 41).

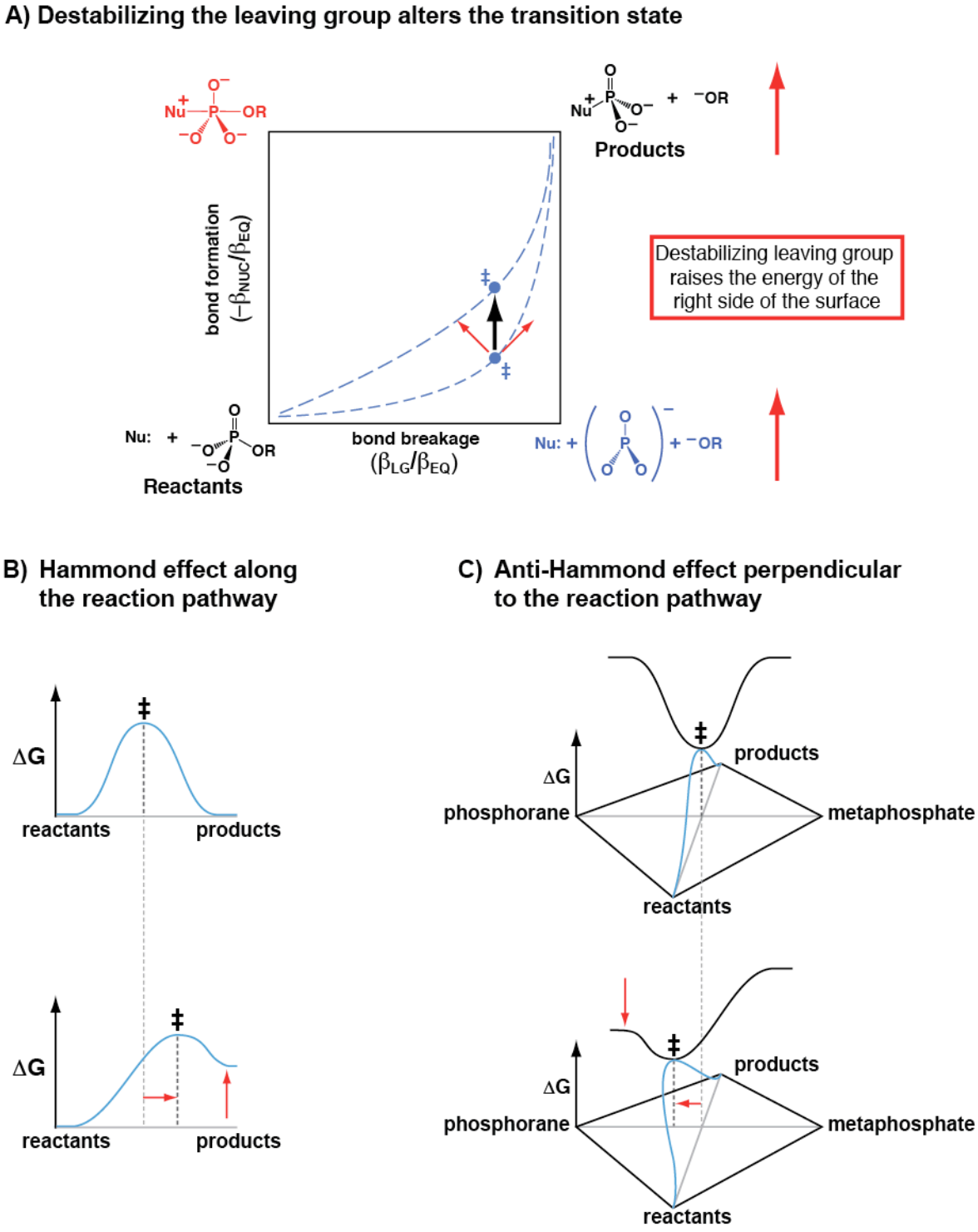

Figure C7. Changes in the transition state predicted with changes in leaving group pK_a. (A) A hypothetical reaction with a loose transition state (blue point). Increasing the pK_a of the leaving group destabilizes the free product and the metaphosphate intermediate, raising two right-side corners of the 2D reaction coordinate diagram. The resulting perturbations of the transition state are composed of vectors governed by (B) Hammond effects and (C) anti-Hammond effects.

D. Linear Free Energy Relationship Data

Phosphate Monoester Dianions and Related Monosubstituted Compounds: β_{NUC}

Table D1. Oxygen nucleophiles with oxygen leaving groups.

Nucleophile series	Leaving group	LG pK_a	Temp. °C	Ionic strength, M	β_{NUC}	Ref
Alcohols	Adenosine diphosphate	6.4	60	0.1	0.07	(42)

Table D2. Oxygen nucleophiles with nitrogen leaving groups.

Nucleophile series	Leaving group	LG pK_a	Temp. °C	Ionic strength, M	β_{NUC}	Ref
Oxygen nucleophiles	Pyridine	5.5	25	1.5	0.24	(38, 43)
Oxygen nucleophiles	γ-picoline	6.3	25	1.5	0.13	(38, 43)
Oxygen nucleophiles	γ-picoline	6.3	25	1.5	0.27	(38, 43)
Oxygen nucleophiles	4-morpholinopyridine	9.0	25	1.5	0.32	(38, 43)

Table D3. Nitrogen nucleophiles with oxygen leaving groups.

Nucleophile series	Leaving group	LG pK_a	Temp. °C	Ionic strength, M	β_{NUC}	Ref
Substituted pyridines	2,4-dinitrophenolate	4.0	39	1	0.0[a]	(44)
Substituted quinuclidines	2,4-dinitrophenolate	4.0	25	1	-0.1[a]	(35)
Amines	Adenosine diphosphate	6.4	65	0.5	0.01	(45)
Substituted quinuclidines	4-nitrophenolate	7.2	25	1	-0.05[a]	(35)

[a] Values of β_{NUC} are reported as given in the paper. These values are likely slightly higher due to a small correction from desolvation of amine nucleophiles (35).

Table D4. Nitrogen nucleophiles with nitrogen leaving groups.

Nucleophile series	**Leaving group**	**LG pK_a**	**Temp. °C**	**Ionic strength, M**	**β_{NUC}**	**Ref**
Substituted pyridines	3-methoxy pyridine	5.1	25	1	0.17	(34, 46)
Primary amines	3-methoxy pyridine	5.1	25	1	0.19	(34)
Substituted pyridines	Isoquinoline	5.5	25	0.2	0.15	(47, 48)
Substituted quinuclidines	Pyridine	5.5	25	1	-0.1 [a]	(35)
amines	4-nitrophenolate	7.2	39	1	0.13	(1)
Primary amines	4-morpholinopyridine	8.5	25	1	0.28	(34)
Substituted quinuclidines	4-morpholinopyridine	8.5	25	1	-0.01 [a]	(35)
Substituted pyridines	4-morpholinopyridine	9.0	25	1	0.22	(34)
Substituted pyridines	Ammonia	9.2	39	1	0.22	(49)

[a] Values of β_{NUC} are reported as given in the paper. These values are likely slightly higher due to a small correction from desolvation of amine nucleophiles (35).

Phosphate Monoester Dianions and Related Monosubstituted Compounds: β_{LG}

Table D5. Oxygen nucleophiles with oxygen leaving groups.

Nucleophile	Nuc. pK_a	Leaving group series	Temp. °C	Ionic strength, M	β_{LG}	Ref.
water	-1.7	Substituted phenols and benzoic acids	39	1.0	-1.23	(2, 50)
water	-1.7	Substituted benzoic acids	39	0.6	-1.16	(50)[a]
water	-1.7	phosphoanhydrides	95	0.1	-1.1	(42)

[a] Value in paper was reported with σ values. See reference (51) for discussion of the σ scale. Here, data were plotted by us using pK_a values from other papers in the table to obtain β_{LG}.

Table D6. Oxygen nucleophiles with nitrogen leaving groups.

Nucleophile	Nuc. pK_a	Leaving group series	Temp. °C	Ionic strength, M	β_{LG}	Ref.
water	-1.7	Substituted pyridines	25	0.2	-1.13	(52)
water	-1.7	Substituted pyridines	25	0.2	-1.11	(47)
Water	-1.7	Substituted pyridines	25	1.5	-1.02	(38, 43)
Phosphate monoanion	1.7	Substituted pyridines	25	1.5	-0.95	(38, 43)
Formate	3.6	Substituted pyridines	25	1.5	-0.98	(38, 43)
Bicarbonate	3.8	Substituted pyridines	25	1.5	-1.0	(38, 43)
Succinate	5.4	Substituted pyridines	25	1.5	-0.96	(38, 43)
Cacodylate	6.2	Substituted pyridines	25	1.5	-0.98	(38, 43)
Phosphate dianion	6.5	Substituted pyridines	25	1.5	-1.0	(38, 43)
Carbonate	9.8	Substituted pyridines	25	1.5	-0.88	(38, 43)
Phosphate trianion	11.4	Substituted pyridines	25	1.5	-0.95	(38, 43)
Trifluoroethoxide	12.4	Substituted pyridines	25	1.5	-0.82	(38, 43)
Hydroxide	15.7	Substituted pyridines	25	1.5	-0.79	(38, 43)

Table D7. Nitrogen nucleophiles with oxygen leaving groups.

Nucleophile	Nuc. pK_a	Leaving group series	Temp. °C	Ionic strength, M	β_{LG}	Ref.
pyridine	5.2	Substituted phenolates	39	1	-1.03	(44)
Triethylenediamine	8.9	Substituted phenolates	39	1	-0.94	(44)

Table D8. Nitrogen nucleophiles with nitrogen leaving groups.

Nucleophile	Nuc. pK_a	Leaving group series	Temp. °C	Ionic strength, M	β_{LG}	Ref.
Pyrazole	2.7	Substituted pyridines	25	0.2	-1.05	(52)
pyridine	5.2	Substituted pyridines	25	0.2	-0.92	(47)
Morpholine	8.4	Substituted pyridines	25	0.2	-0.96	(52)
Triethylenediamine	8.9	Substituted pyridines	25	0.2	-0.99	(52)
Ammonia	9.2	Substituted pyridines	25	0.2	-0.97	(52)
methylamine	10.6	Substituted pyridines	25	0.2	-0.88	(52)

Phosphate Monoester Dianions and Related Monosubstituted Compounds: β_{EQ}

Table D9. β_{EQ} estimates

Nucleophiles	Leaving groups	Temp. °C	Ionic strength, M	β_{EQ}	Reference
Pyridines	Pyridines	25	1	-1.05	(34)
pyridines	Pyridines	25	0.2	- 1.07	(47)
water	Mixed oxygen leaving groups	25	1[a]	-1.35	(33)

[a] Data from a variety of conditions were used.

Phosphate Diesters and Related Disubstitued Compounds:

β_{NUC}

Table D10. Oxygen nucleophiles with oxygen leaving groups.

Nucleophile series	Leaving group	Leaving group pK_a	R'	Temp. °C	Ionic strength, M	β_{NUC}	Ref.
Oxygen nucleophiles	2,4-dinitrophenolate	4.1	Methyl	39	1	0.31	(53)

Table D11. Nitrogen nucleophiles with oxygen leaving groups.

Nucleophile series	Leaving group	Leaving group pK_a	R'	Temp. °C	Ionic strength, M	β_{NUC}	Ref.
Substituted pyridines	2,4-dinitrophenolate	4.1	Methyl	39	1	0.31[a]	(53)
Primary amines	2,4-dinitrophenolate	4.1	Methyl	39	1	0.31	(53)
Substituted pyridines	2,4-dinitrophenolate	4.1	2,4-dinitrophenolate	39	1	0.54	(44)
Substituted pyridines	2,4-dinitrophenolate	4.1	Methyl	23	1.7	0.56	(54)
Substituted pyridines	2,4-dinitrophenolate	4.1	Methyl	39	1	0.44[a]	(53, 54)
Substituted pyridines	4-acetyl-2-nitrophenolate	5.1	Methyl	39	1	0.33	(53)
Substituted pyridines	4-chloro-2-nitrophenolate	6.4	Methyl	39	1	0.35	(53)
Substituted pyridines	4-nitrophenolate	7.2	Methyl	39	1	0.38	(53)

[a] Value of 0.31 reported in the 1970 paper (53); a later paper (54) reported a value of 0.44 from analysis of the same dataset.

Phosphate Diesters and Related Disubstituted Compounds:

β_{LG}

Table D12. Oxygen nucleophiles with oxygen leaving groups.

Nucleophile	Nucleophile pK_a	Leaving group series	R'	Temp °C	Ionic strength, M	β_{LG}	Ref.
water	-1.7	aryl	aryl	100	1	-0.97	(4)[a]
water	-1.7	aryl	aryl	39	1	-1.16	(4, 55)
phenolate	10.0	aryl	methyl	39	1	-0.64	(56)
hydroxide	15.7	phenolates	methyl	25	1	-0.94	(57)
hydroxide	15.7	mixed	mixed	25	1	-0.76	(5)
hydroxide	15.7	phenolates	methyl	25	0.1	-0.64	(58)[b]

[a] The R' substituent was varied in the LFER experiment in addition to the leaving group. Some rate constants may be overestimates because pH-independent reactions were slow.
[b] Value includes a data point for dimethyl phosphate hydrolysis, later found to be an overestimate (59).

Table D13. Nitrogen nucleophiles with oxygen leaving groups.

Nucleophile	Nucleophile pK_a	Leaving group series	R'	Temp °C	Ionic strength, M	β_{LG}	Ref.
Pyridine	5.2	phenolates	Methyl	39	1	-1.06	(53)
3-picoline	5.6	phenolates	methyl	23	1.7	-1.3	(54)
4-methylpyridine	5.7	phenolates	Methyl	39	1	-1.03	(53)
4-aminopyridine	9.2	phenolates	Methyl	39	1	-0.98	(53)

Table D14. Intramolecular reactions, oxygen nucleophiles and leaving groups.

Nucleophile	Nucleophile pK_a	Leaving group series	R'	Temp °C	Ionic strength, M	β_{LG}	Ref.
2' hydroxyl, intramolecular, hydroxide-catalyzed	~13	phenolates	uridine	25	0.25	-0.54	(60)
2' hydroxyl, intramolecular, imidazole-catalyzed	~13	phenolates	uridine	25	0.25	-0.59	(60)
2' hydroxyl, intramolecular, hydroxide-catalyzed	~13	alkyl	uridine	25	1	-1.28	(61)
2' hydroxyl, intramolecular	~13	phenolates	guanosine	35	0.2	-0.87	(62)
Hydroxyalkyl, intramolecular	~13	mixed	hydroxypropyl	80	0.5	-0.56	(63)

Phosphate Diesters and Related Disubstitued Compounds:

β_{EQ}

Table D15. β_{EQ} estimates.

Nucleophiles	Leaving groups	R',R"	Temp. °C	Ionic strength, M	β_{EQ}	Reference
water	Mixed oxygen LG	Estimated from H	25	1[a]	-1.73	(33)
Estimated for phenolates	pyridines	Estimated for CH_3	Estimated for 23	Estimated for 1.7 M	-1.6	(54)
-	pyridines	-	-	-	-1.4	(33, 34)[b]

[a] Data from a variety of conditions were used.

[b] Estimated by starting with the β_{EQ} value for nitrogen nucelophiles with monoesters (-1.05) and accounting for a difference of 0.38 upon protonation of the nonbridging oxygen (33, 34).

Phosphate Triesters:
β_{NUC}

Table D16. Oxygen nucleophiles with oxygen leaving groups.

Nucleophile series	Leaving group	Leaving group pK_a	R',R"	Temp. °C	Ionic strength, M	β_{NUC}	Ref.
Oxygen nucleophiles	2,4-dinitrophenolate	4.1	Alkyl, cyclic	39	1	0.30	(55)
Oxygen nucleophiles	2,4-dinitrophenolate	4.1	Benzyl	30	1	0.37 [a]	(64)
Oxygen nucleophiles	2,4-dinitrophenolate	4.1	Alkyl, cyclic	25	1	0.49	(29)
Substituted phenolates	2,4-dinitrophenolate	4.1	Aryl	25	0.5	0.12	(36)
Oxygen nucleophiles	4-acetyl-2-nitrophenolate	5.1	Alkyl, cyclic	39	1	0.37	(55)
Oxygen nucleophiles	4-chloro-2-nitrophenolate	6.5	Alkyl, cyclic	39	1	0.42	(55)
Oxygen nucleophiles	4-nitrophenolate	7.1	Alkyl, cyclic	39	1	0.48	(55)
Substituted phenolates	4-nitrophenolate	7.1	Aryl	25	0.5	0.53	(36)
Oxygen nucleophiles	4-nitrophenolate	7.1	Alkyl, cyclic	25	1	0.64	(29)
phenolates	4-nitrophenolate	7.1	aryl	25	0.5	0.53	(65)
Oxygen nucleophiles	phenolate	10.0	Alkyl, cyclic	25	1	0.75	(29)

[a] Fit of line to all points.

Phosphate Triesters:
β_{LG}

Table D17. Oxygen nucleophiles with oxygen leaving groups.

Nucleophile	Nucleophile pK_a	Leaving group series	R',R"	Temp. °C	Ionic strength, M	β_{LG}	Ref.
water	-1.7	Substituted phenolate	Alkyl, cyclic	39	1	-0.99	(55)
Acetate	4.8	Substituted phenolate	Alkyl, cyclic	39	1	-0.88	(55)
acetate	4.8	Substituted phenolate	Alkyl, cyclic	25	1	-0.75	(29)
Phosphate dianion	7.2	Substituted phenolate	Alkyl, cyclic	39	1	-0.65	(55)
Phosphate	7.2	Substituted phenolate	Alkyl, cyclic	25	1	-0.62 [b]	(29)
4-formylphenolate	7.7	Substituted phenolate	Aryl	25	0.5	-0.81	(36)
4-acetylphenolate	8.1	Substituted phenolate	Aryl	25	0.5	-0.68	(36)
Hexafluoroisopropoxide	9.3	Substituted phenolate	Alkyl, cyclic	25	1	-0.61 [a, b]	(29)
phenolate	10.0	Substituted phenolate	Aryl	25	0.5	-0.52	(36)
phenolate	10.0	Substituted phenolate	ethyl	39	1	-0.51	(56)
Carbonate	10.3	Substituted phenolate	Alkyl, cyclic	39	1	-0.54	(55)
Hydroperoxide	11.6	Substituted phenolate	Alkyl, cyclic	39	1	-0.35	(55)
Triflouroethoxide	12.4	Substituted phenolate	Alkyl, cyclic	39	1	-0.34	(55)
trifluoroethoxide	12.4	Substituted phenolate	Alkyl, cyclic	25	1	-0.45 [a, b]	(29)
hydroxide	15.7	Substituted phenolate	Aryl	25	0.5	-0.55	(36)
hydroxide	15.7	Substituted phenolate	Alkyl, cyclic	25	1	-0.37 [a, b]	(29)
Hydroxide	15.7	Substituted phenolate	Alkyl, cyclic	39	1	-0.41	(55)
hydroxide	15.7	Substituted phenolates	ethyl	25	1	-0.5 [c]	(66)
hydroxide	15.7	Substituted phenolates	ethyl	25	1	-0.43	(67)

[a] averaged axial and equatorial values
[b] reaction may proceed in stepwise manner (29)
[c] pseudo-first order rate constants in 1 M KOH.

Phosphate Triesters:

β_{EQ}

Table D18. β_{EQ} estimates

Nucleophiles	Leaving groups	R',R"	Temp. °C	Ionic strength, M	β_{EQ}	Reference
phenolate	phenolate	Aryl	25	0.5	-1.3	(36)
Oxygen nucleophiles	phenolates	Alkyl, cyclic	25	1	-1.2	(29)
phenolate	phenolates	ethyl	39	1	-1.83	(56)
phenolates	phenolates	aryl	25	0.5	-1.4	(65)
water	Mixed oxygen LG	Estimated from H	25	1[a]	-1.82	(33)

[a] Data from a variety of conditions were used.

E. Thio-substituted Compounds: Rate Effects and LFER Data

As discussed in the main text, thio-substituted phosphate esters, or phosphorothioates (where S is substituted at a nonbridging position) and phosphorothiolates (where S is substituted at a bridging position) provide useful mechanistic comparisons for investigation of catalyzed and uncatalyzed phosphoryl transfer. In this section, we focus on rate effects and LFER data for phosphorothioates, which have provided important perspective in studies of the nonenzymatic transition state structures for phosphoryl transfer reactions. Section F discusses KIE data for these compounds. For further reading on mechanistic studies of phosphorothiolates (with bridging S-substitution), see, for example, references (54, 67, 68).

Phosphorothioate monoesters

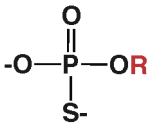

Nonenzymatic reactions of phosphorothioate monoesters are around an order of magnitude faster than those of the corresponding phosphate monoesters (6, 69). For example, 4-nitrophenyl phosphorothioate dianion reacts with water 13-fold faster than 4-nitrophenyl phosphate dianion at 39 °C (6).

LFER data suggest that reactions of phosphorothioate monoester dianions and phosphate monoester dianions have similar transition states. A value of -1.1 for β_{LG} for O-aryl phosphorothioates has been reported (70), similar to values of -1.2 reported in Table D5 for phosphate monoester dianions. As discussed in the main text and in Supplemental Section B, stereochemical racemization has been observed in reactions of phosphorothioate monoesters, suggesting the formation of freely diffusing thiometaphosphate as an intermediate subsequent to the loose transition state (15, 16). This observation, and the increase in rates observed upon thio-substitution, are consistent with the idea that thio-substitution can stabilize the metaphosphate intermediate, as discussed in the main text.

Phosphorothioate diesters

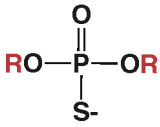

In contrast to the observations for phosphate monoesters, reactions of phosphorothioate diesters are around an order of magnitude slower than those of the corresponding phosphate diesters. Differences in nonenzymatic reactivity between phosphorothioate and phosphate aryl methyl diesters have been measured with a series of different nucleophiles, giving a range of thio-effects from 4- to 11-fold and an average thio-effect of about 7-fold (7). This observed change in direction of thio-effects from monoester to diester reactions is consistent with tighter transition states for diester reactions, as thio-substitution may stabilize free metaphosphate but may have a destabilizing effect on more phosphorane-like transition states. The cleavage of RNA via intramolecular attack of a neighboring 2'-oxyanion gives a thio-effect of one –i.e., a rate

indistinguishable from that of normal oxygen-containing RNA (71); the origin of the difference relative to the reactions noted above remains to be elucidated.

LFER data for some phosphorothioate diester reactions have also been measured. Values of β_{LG} have been measured for intramolecular transesterification reactions of uridine 3'-aryl phosphorothioates catalyzed by hydroxide (β_{LG} = -0.55) and imidazole (β_{LG} = -0.63) (72). These values are similar to those reported for 3'-aryl phosphates, β_{LG} = -0.54 for hydroxide-catalyzed reactions and β_{LG} = -0.59 for imidazole-catalyzed reactions (60), as reported in Table D14.

Phosphorothioate triesters

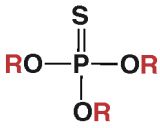

Consistent with a continuing trend from monoester to diester reactions, reactions of phosphorothioate triesters range from one to two orders of magnitude slower than those of phosphate triesters (67, 73, 74). For example, the hydroxide-mediated reactions of aryl diethyl phosphorothioate triesters are approximately an order of magnitude slower than those of aryl diethyl phosphate triesters (67). Leaving group LFER data reported for aryl diethyl phosphate and phosphorothioate triesters are similar, with β_{LG} = -0.35 and β_{LG} = -0.43, respectively, suggesting similar transition states (67).

Table E1. β_{LG} data for thio-substituted compounds.

Reaction	**Nucleophile**	**nucleophile pK_a**	**Leaving group series**	**Temp. °C**	**Ionic strength, M**	**β_{LG}**	**Ref**
Phosphorothioate **monoester** dianions	water	-1.7	phenolates	25	1	-1.1	(70)
Nucleotide phosphorothioate **diesters,** Intramolecular transesterification, hydroxide-catalyzed	2' hydroxyl, intramolecular transesterification	~13	phenolates	25	0.25	-0.55	(72)
Nucleotide phosphorothioate **diesters**, Intramolecular transesterification, imidazole-catalyzed	2' hydroxyl, intramolecular transesterification	~13	phenolates	25	0.25	-0.63	(72)
Diethyl phosphorothioate **triesters**	hydroxide	15.7	phenolates	25	1	-0.35	(67)

F. Kinetic Isotope Effects for Phosphoryl and Sulfuryl Transfer Reactions

Table F1. Compounds and abbreviations

Phosphate Monesters	
pNPP	*p*-nitrophenyl phosphate
mNBP	*m*-nitrobenzyl phosphate
pNPP-S	*p*-nitrophenyl phosphorothioate
Phosphate Diesters	
EtOpNPP	Ethyl *p*-nitrophenyl phosphate
EtOpNPP-S	Ethyl *p*-nitrophenyl phosphorothioate
ptBuPpNPP	*p*-*tert*-butylphenyl *p*-nitrophenyl phosphate
dMeBupNPP	3,3-dimethyl *p*-nitrophenyl phosphate
T5-pNPP	Thymidine-5′-*p*-nitrophenyl phosphate
Phosphate Triesters	
$(EtO)_2$pNPP	Diethyl *p*-nitrophenyl phosphate (paraoxon)
$(EtO)_2$(4-carbamoyl)PP	Diethyl 4-carbamoyl phenylphosphate
$(EtO)_2$mNBP	Diethyl *m*-nitrobenzyl phosphate
$(EtO)_2$PC	Diethyl phosphorylcholine
$(MeO)_2$pNPP-S	Dimethyl *p*-nitrophenyl phosphorothioate
Sulfate Esters	
pNPS	*p*-nitrophenyl sulfate
PpNPS	Phenyl *p*-nitrophenyl sulfate

Sites of labeling for leaving group KIEs

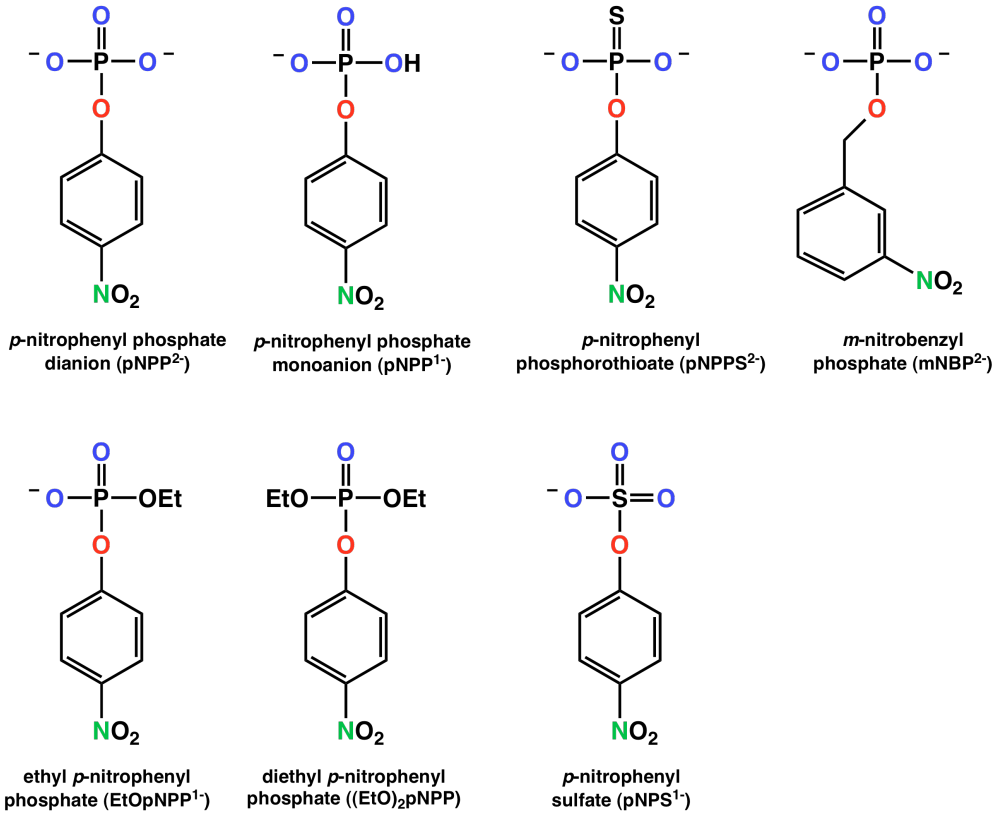

Reaction of a phosphate monoester dianion

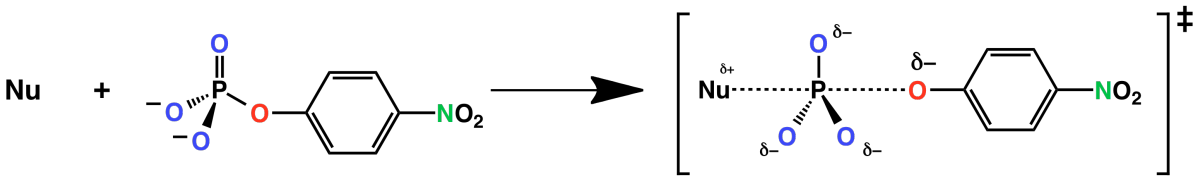

Figure F1. Representative phosphate and sulfate ester compounds, with sites of isotope labeling shown in color.

Presentation of the KIE Data

The tables below compile KIE data from the literature for phosphoryl transfer reactions. For comparison, reactions of thio-substituted phosphate esters (phosphorothioates) and sulfate esters are included. Phosphorothioates are listed in *italics*. These compounds behave similarly to their corresponding phosphate esters, with occasional minor differences (as discussed in the main text).

Leaving group KIEs for the bridging oxygen (Figure F1, red), nonbridging oxygen(s) (Figure F1, blue), and remote label nitrogen (Figure F1, green) are reported as $^{18}k_{bridge}$, $^{18}k_{nonbridge}$, and ^{15}k respectively for nonenzymatic reactions and as $^{18}(V/K)_{bridge}$, $^{18}(V/K)_{nonbridge}$, and $^{15}(V/K)$ respectively for enzymatic reactions (75). (V/K) indicates that the KIE was determined by competition between labeled and unlabeled substrates, and is thus an observed isotope effect on the bimolecular rate constant k_{cat}/K_M.

Values of $^{18}k_{nonbridge}$ are reported both as the total observed effect and per-oxygen-atom to facilitate comparisons between compounds that have differing numbers of nonbridging oxygen atoms. For phosphate monoesters with three nonbridging oxygen atoms, the per-oxygen-atom effect is the cube root of the total observed effect. For diesters with two nonbridging oxygen atoms, the per-oxygen-atom effect is the square root of the total observed effect. KIEs for nucleophilic attack ("Nu" in Figure F1) are reported as $^{18}k_{nuc}$. For some compounds, certain KIEs were not determined (n.d.) or, in the case of some remote ^{15}N labels, not reported (n.r.).

Nonenzymatic Reactions

Nonenzymatic Phosphate Monoester Hydrolysis

In alkaline conditions, the predominant form of a phosphate monoester is dianionic (Figure F1), and the dependence of the reaction rate on pH suggests that neutral water, not hydroxide, is the attacking nucleophile (2). The primary KIEs ($^{18}k_{bridge}$) for hydrolysis of phosphate monoester dianions are large and normal, suggesting a loose transition state with extensive bond cleavage to the leaving group (76-78). Small normal values of ^{15}k reflect bond cleavage and negative charge delocalization into the leaving group (75). Because changes in geometry as well as bonding affect vibrational modes and the corresponding KIEs, the values for nonbridging oxygen atoms are challenging to predict. The observed values of $^{18}k_{nonbridge}$ are small and inverse for phosphate monoesters (78), suggesting that a potential normal effect arising from hybridization changes is outweighed by an inverse contribution from bond order changes (75). In contrast, the large, normal value of $^{18}k_{nonbridge}$ for pNPP-S^{2-} suggests a dominant contribution from loosening bending modes in the transition state for phosphorothioate monoester hydrolysis (79).

Table F2

	^{15}k	$^{18}k_{bridge}$	$^{18}k_{nonbridge}$	$^{18}k_{nonbridge}$ (per O)	Ref
pNPP^{2-} (95 °C)	1.0028 ± 0.0002	1.0189 ± 0.0005	0.9994 ± 0.0005	0.9998	(78)
pNPP^{2-} (35 °C) t-butanol	1.0039 ± 0.0003	1.0202 ± 0.0008	0.9997 ± 0.0016	0.9999	(78)
pNPP-S^{2-} (35 °C)	*1.0027 ± 0.0001*	*1.0237 ± 0.0007*	*1.0135 ± 0.0013*	*1.0067*	*(79)*

In acidic conditions, phosphate monoesters are monanionic (Figure F1). KIEs for hydrolysis of phosphate monoester monoanions such as $pNPP^{1-}$ and $mNBP^{1-}$ suggest a loose transition state, similar to that for dianion hydrolysis, with proton transfer from the phosphoryl group to the leaving group in the transition state (2, 78, 80, 81). Relative to the KIEs for dianion hydrolysis, there is a normal contribution to $^{18}k_{nonbridge}$ from loss of the proton, and an inverse contribution to $^{18}k_{bridge}$ from protonation of the leaving group oxygen atom.

Table F3

	^{15}k	$^{18}k_{bridge}$	$^{18}k_{nonbridge}$	$^{18}k_{nonbridge}$ **(per O)**	**Ref**
$pNPP^{1-}$ (95 ˚C)	1.0004 ± 0.0002	1.0087 ± 0.0003	1.0184 ± 0.0005	1.0061	(78)
$pNPP^{1-}$ (30 ˚C)	1.0005 ± 0.0001	n.d.	1.0199 ± 0.0003	1.0066	(82)
$mNBP^{1-}$ (115 ˚C)	1.0000 ± 0.0001	1.0157 ± 0.0009	1.0151 ± 0.0002	1.0050	(80, 81)
pNPP-S^{1-} (50 ˚C)	*1.0005 ± 0.0001*	*1.0091 ± 0.0007*	*1.0221 ± 0.0004*	*1.0110*	*(79)*

Although phosphate monoester dianions react with neutral water under alkaline conditions, the diesters and triesters discussed below react with hydroxide under alkaline conditions. This difference in principle presents a problem for comparing KIE values between monoesters, diesters, and triesters. In practice, however, linear free energy relationship data suggest that the transition state for monoester hydrolysis is largely insensitive to the identity of the nucleophile (38).[1] Thus, comparisons can be made between monoester reactions with water and the reactions of diesters and triesters with hydroxide described below.

Nonenzymatic Phosphate Diester Hydrolysis

In alkaline conditions, phosphate diester monoanions react with hydroxide (4, 53, 83). Phosphate diesters exhibit smaller values of $^{18}k_{bridge}$ and ^{15}k than observed for monoesters, suggesting a transition state that is intermediate between the loose and tight extremes (79, 83, 84). Values of $^{18}k_{nonbridge}$ vary from small and inverse to small and normal.

Table F4

	^{15}k	$^{18}k_{bridge}$	$^{18}k_{nonbridge}$	$^{18}k_{nonbridge}$ **(per O)**	**Ref**
$EtOpNPP^{1-}$ (95 ˚C)	1.0010 ± 0.0001	1.0042 ± 0.0009	0.9974 ± 0.0006	0.9986	(79)[a]
EtOpNPP-S^{1-} (95 ˚C)	*1.0010 ± 0.0002*	*1.0020 ± 0.0006*	*1.0019 ± 0.0004*	*1.0019*	*(79)*
$ptBuPpNPP^{1-}$ (70 ˚C)	1.0010 ± 0.0001	1.0046 ± 0.0008	1.0040 ± 0.0001	1.0020	(83)
$dMeBupNPP^{1-}$ (95 ˚C)	1.0016 ± 0.0002	1.0059 ± 0.0005	0.9949 ± 0.0006	0.9974	(83)

[a] $^{18}k_{nonbridge}$ for $EtOpNPP^{1-}$ is an unpublished value from E.A. Tanifum & A.C. Hengge.

[1] Specifically, there is only a small difference between the values of β_{lg} for monoester reactions with neutral water versus hydroxide, corresponding to a small p_{xy} coefficient.

In acidic conditions, phosphate diesters are predominantly neutral, and the KIEs suggest proton transfer in the transition state, analogous to the situation with phosphate monoester monoanions.

Table F5

	^{15}k	$^{18}k_{bridge}$	$^{18}k_{nonbridge}$	$^{18}k_{nonbridge}$ (per O)	Ref
ptBuPpNPP (95 ˚C)	1.0007 ± 0.0001	1.0058 ± 0.0005	1.0088 ± 0.0002	1.0044	(83)
dMeBupNPP (95 ˚C)	1.0009 ± 0.0002	1.0039 ± 0.0004	1.0139 ± 0.0004	1.0069	(83)

The KIE for nucleophilic attack on the diester T5-pNPP (Table F1) has been measured using methods that allow direct measurement of $^{16}O/^{18}O$ ratios (85). KIEs for nucleophilic attack include an inverse contribution from bond formation in the transition state and a normal contribution from reaction coordinate motion (86, 87). In the case of hydroxide attack on T5-pNPP, the normal contribution from reaction coordinate motion is dominant, and the data suggest direct attack by hydroxide in the transition state. Combined with the small, normal leaving group KIEs, these data support a concerted mechanism for phosphate diester hydrolysis with simultaneous nucleophilic attack and departure of the leaving group.

Table F6

	Nucleophile	$^{18}k_{nuc}$	Ref
T5-pNPP $^{1-}$ (37 ˚C)	HO^-	1.027 ± 0.010	(85)

Nonenzymatic Phosphate Triester Hydrolysis

Phosphate triesters are neutral over a wide range of pH values. The KIEs listed below were determined under alkaline conditions, where the attacking nucleophile is hydroxide. Values of $^{18}k_{bridge}$ are normal with a magnitude that crudely correlates with decreasing leaving group pK_a. One possible interpretation of this data is that the extent of bond cleavage increases for poorer leaving groups (37, 88). An alternative interpretation has been suggested (89), in which the normal contribution to primary KIEs from reaction coordinate motion (86, 87) becomes significant due to coupling between the stretching frequencies of the nucleophile and leaving group. This coupling was suggested to become more significant as the leaving group pK_a approaches that of the hydroxide nucleophile, leading to a more symmetrical transition state (89). Values of $^{18}k_{nonbridge}$ are large and normal, suggesting significant nucleophilic participation in the transition state, consistent with results from LFERs measuring β_{NUC} (55).

Table F7

	^{15}k	$^{18}k_{bridge}$	$^{18}k_{nonbridge}$	$^{18}k_{nonbridge}$ (per O)	Ref
$(EtO)_2$pNPP (25 ˚C)	1.0007 ± 0.0001	1.0060*	1.0063 ± 0.0001	1.0063	(77, 88)
$(EtO)_2$(4-carbamoyl)PP (25 ˚C)	n.r.	1.027 ± 0.002	1.025 ± 0.002	1.025	(88)
$(EtO)_2$mNBP	n.r.	1.052 ± 0.003	n.d.	n.d.	(89)
$(EtO)_2$PC	n.r.	1.041 ± 0.003	1.033 ± 0.002	1.033	(89)
$(MeO)_2$pNPP-S (30 ˚C)	*1.0004 ± 0.0002*	*1.0045 ± 0.0006*	*n.d.***	*n.d.***	*(79)*

*No error estimate is available for this measurement.
**There are no nonbridging oxygen atoms in this molecule.

Nonenzymatic Sulfate Ester Hydrolysis

Sulfate monoesters are monoanionic over a broad range of pH values and react with neutral water (90). Values of the KIEs for sulfate monoester hydrolysis are similar to those for phosphate monoester dianions, and suggest a similar loose transition state with extensive bond cleavage to the leaving group.

Table F8

	^{15}k	$^{18}k_{bridge}$	$^{18}k_{nonbridge}$	$^{18}k_{nonbridge}$ (per O)	Ref
$pNPS^{1-}$ (85 ˚C)	1.0026 ± 0.0001	1.0210 ± 0.0010	0.9951 ± 0.0003	0.9984	(90)

In acidic conditions, the neutral form of the sulfate monoester becomes more reactive than the monoanion (90). The KIEs for hydrolysis of the neutral sulfate monoester are similar to those for phosphate monoester monoanions, and suggest proton transfer from the sulfuryl group to the leaving group in the transition state.

Table F9

	^{15}k	$^{18}k_{bridge}$	$^{18}k_{nonbridge}$	$^{18}k_{nonbridge}$ (per O)	Ref
pNPS (65 ˚C)	1.0002 ± 0.0001	1.0069 ± 0.0002	1.023*	1.0076	(90)

*The value of $^{18}k_{nonbridge}$ for neutral pNPS is estimated from the observed KIE in acidic conditions and the fractionation factor for protonation of pNPS.

The value of $^{18}k_{bridge}$ for the sulfate diester PpNPS is significantly smaller than that for the sulfate monoester pNPS, suggesting a tighter transition state, analogous to how the transition states for phosphate diesters and triesters are tighter than those for phosphate monoesters.

Table F10

	^{15}k	$^{18}k_{bridge}$	$^{18}k_{nonbridge}$	$^{18}k_{nonbridge}$ (per O)	Ref
PpNPS	1.0000 ± 0.0005	1.003 ± 0.002	n.d.	n.d.	(91)

Enzymatic Reactions

Below we survey a few particularly instructive examples from the vast body of literature reporting KIEs for enzyme-catalyzed phosphoryl transfer reactions. The enzymes discussed below include alkaline phosphatase, protein tyrosine phosphatase, and Ras GTPase. KIE data of potential interest that are not discussed herein include leaving group KIEs for Ser/Thr protein phosphatases (92-95), hexokinase (96), kanamycin nucleotidyltransferase (97), RNase A (98), and phosphotriesterase (88), and a value of $^{18}k_{nuc}$ for the RNase P ribozyme (99).

Alkaline Phosphatase Reactions

Alkaline phosphatase (AP) catalyzes the hydrolysis of phosphate monoester dianions. AP also catalyzes the hydrolysis of phosphorothioate and sulfate monoesters, and these values are included for comparison. Because some reactions of wild type (wt) AP are not limited by the chemical step, KIE data were also collected for a mutant, R166S AP, for which reactions are limited by chemistry. For wt AP, KIEs for the reaction of $pNPP^{2-}$ are near unity, consistent with a nonchemical rate-determining step (78, 100), and reactions of $mNBP^{2-}$ are likely to be partially limited by a nonchemical step (101). Values of $^{18}(V/K)_{bridge}$ for all other reactions of wt and R166S AP are large and normal, although smaller than the values of $^{18}k_{bridge}$ for corresponding nonenzymatic reactions. These results could be taken to suggest a tighter transition state for AP-catalyzed phosphate monoester hydrolysis than that in solution. This interpretation is inconsistent, however, with the observation that values of $^{18}(V/K)_{nonbridge}$ are smaller (more inverse) than the corresponding values of $^{18}k_{nonbridge}$, as a tighter transition state would be expected to give more normal values of $^{18}(V/K)_{nonbridge}$.

An alternative, consistent interpretation of the KIE data is that AP catalyzes phosphate monoester hydrolysis through a loose transition state, similar to that in solution, and the inverse contributions to both $^{18}(V/K)_{bridge}$ and $^{18}(V/K)_{nonbridge}$ are the result of interactions with active site Zn^{2+} ions (101). This interpretation is consistent with a large body of LFER data suggesting that the transition state for AP-catalyzed phosphate monoester hydrolysis is loose, similar to that in solution (70, 100, 102-104).

One exception to the trend in the $^{18}(V/K)_{nonbridge}$ KIEs noted above is that for the sulfate monoester $pNPS^{1-}$. While the value of $^{18}(V/K)_{bridge}$ is reduced relative to $^{18}k_{bridge}$, consistent with an inverse contribution from an active site Zn^{2+} ion, the value of $^{18}(V/K)_{nonbridge}$ for $pNPS^{1-}$ is indistinguishable from $^{18}k_{nonbridge}$ (105). If active site Zn^{2+} interactions with the nonbridging oxygen atoms lead to an inverse contribution to the KIEs for phosphate monoester reactions and for the leaving group in sulfate monoester reactions, why is a similar effect not observed for the nonbridging oxygen atoms of $pNPS^{1-}$? A key difference between AP-catalyzed reactions of phosphate and sulfate monoesters is that the catalytic proficiency for phosphate monoester reactions is substantially greater than that for sulfate monoester reactions, and this difference has been attributed to differing electrostatic interactions between nonbridging oxygen atoms and the active site Zn^{2+} ions (10). Thus, the interaction between the active site Zn^{2+} ions and the nonbridging oxygen atom of a sulfate monoester, which has less negative charge than that for a phosphate monoester, may be too weak to lead to a significant inverse contribution to $^{18}(V/K)_{nonbridge}$ (105).

Table F11. Wt AP-Catalyzed Reactions

	$^{15}(V/K)$	$^{18}(V/K)_{bridge}$	$^{18}(V/K)_{nonbridge}$	Ref
$pNPP^{2-}$	1.0003 ± 0.0002	1.0003 ± 0.0004	0.9982 ± 0.0001	(78)
$mNBP^{2-}$	0.9999 ± 0.0004	1.0072 ± 0.0007	0.9988 ± 0.0004	(101)
pNPP-S^{2-}	*1.0005 ± 0.0002*	*1.0094 ± 0.0004*	*0.9760 ± 0.0022*	*(101)*
$pNPS^{1-}$	1.0019 ± 0.0004	1.0084 ± 0.0010	0.9946 ± 0.0004	(105)

Table F12. R166S AP-Catalyzed Reactions

	$^{15}(V/K)$	$^{18}(V/K)_{bridge}$	$^{18}(V/K)_{nonbridge}$	Ref
$pNPP^{2-}$	1.0007 ± 0.0001	1.0091 ± 0.0006	0.9925 ± 0.0011	(105)
$mNBP^{2-}$	n.d.	1.0199 ± 0.0013	0.9933 ± 0.0004	(101)
pNPP-S^{2-}	*1.0006 ± 0.0001*	*1.0098 ± 0.0003*	*0.9768 ± 0.0025*	*(101)*

Protein Tyrosine Phosphatase Reactions

Protein tyrosine phosphatases (PTPs) catalyze the hydrolysis of phosphorylated tyrosine residues. KIE data have been collected for PTPs from many different species and from a variety of mutants (75, 106-108). Here we highlight a representative set of KIE data collected for the PTP from *Yersinia*, which has been a model system for studies on PTP mechanism (109). KIEs for wt *Yersinia*-PTP catalyzed $pNPP^{2-}$ hydrolysis are similar to values for $pNPP^{2-}$ hydrolysis in solution and consistent with a loose transition state for the enzymatic reaction. The PTP active site contains a general acid (Asp356) that protonates the leaving group. When this general acid is mutated, the value of $^{18}(V/K)_{bridge}$ increases significantly, suggesting that the leaving group is protonated in the transition state, and that the value of $^{18}(V/K)_{bridge}$ for the wt enzyme reflects a normal contribution from bond breaking and an inverse contribution from protonation of the leaving group oxygen atom.

Table F13. PTP-Catalyzed Reactions

Substrate	Enzyme	$^{15}(V/K)$	$^{18}(V/K)_{bridge}$	$^{18}(V/K)_{nonbridge}$	Ref
$pNPP^{2-}$	Wt	0.9999 ± 0.0003	1.0160 ± 0.0015	1.0001 ± 0.0013	(109)
$pNPP^{2-}$	D356N	1.0024 ± 0.0005	1.0275 ± 0.0016	1.0022 ± 0.0005	(109)
$pNPP^{2-}$	D356A	1.0022 ± 0.0003	1.0274 ± 0.0008	1.0007 ± 0.0005	(109)

Ras GTPase Reactions

Ras is a G protein that hydrolyzes GTP to produce GDP and inorganic phosphate. The Ras-catalyzed GTPase reaction is accelerated by a GAP (GTPase activating protein), which plays an important role in regulating G protein signaling. KIEs for Ras and Ras-GAP catalyzed GTP hydrolysis have been determined using a ^{13}C remote label in the guanosine base (110, 111), in contrast to the leaving group KIEs reported above, which were measured using a ^{15}N remote label in the leaving group. The values of $^{18}(V/K)$ for the leaving group [$^{18}(V/K)_{LG}$] differs from the values of $^{18}(V/K)_{bridge}$ reported above in that $^{18}(V/K)_{LG}$ was determined with three ^{18}O oxygen labels at the β position (Figure F2), which reflects the extent of cleavage of the P_γ-$O_{\beta\gamma}$ bond (111). The large, normal values of $^{18}(V/K)_{LG}$ suggest extensive bond cleavage to the leaving group, consistent with a loose transition state. Values of $^{18}(V/K)_{nonbridge}$ are close to unity, similar with the values observed for $^{18}k_{nonbridge}$ for phosphate monoester hydrolysis reactions in solution (Table F2), and again consistent with a loose transition state for Ras-catalyzed GTP hydrolysis.

GTP Hydrolysis

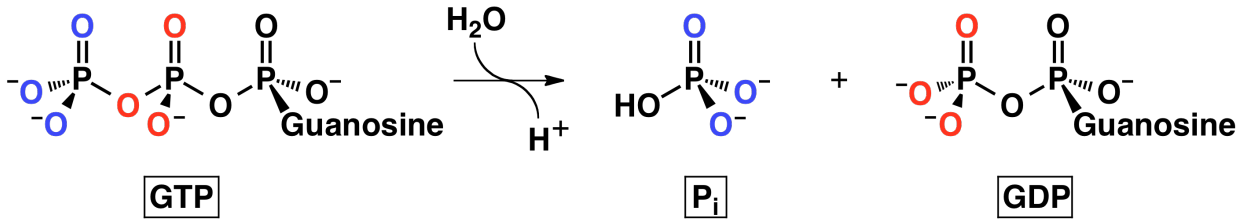

Figure F2. Sites of isotopic labeling in GTP. The leaving group oxygen atoms ($\gamma^{18}O_3$) are shown in red, and the nonbridging oxygen atoms ($\beta^{18}O_3$) are shown in blue.

Table F14. Ras-Catalyzed Reactions

Substrate	**Enzyme**	**$^{18}(V/K)_{LG}$ ($\beta^{18}O_3$)**	**$^{18}(V/K)_{nonbridge}$ ($\gamma^{18}O_3$)**	**Ref**
GTP	Ras	1.0192 ± 0.0005	0.9994 ± 0.0009	(111)
GTP	Ras-GAP	1.0220 ± 0.0014	1.0012 ± 0.0011	(111)

G. Volumes and Entropies of Activation

The volume of activation of a reaction, $\Delta V^{\ddagger}$, is a measure of change in volume between the ground state and the transition state. Activation volumes are obtained by measuring the pressure dependence of the rate constant for a reaction at constant temperature, as follows (112-119):

$$\Delta V^{\ddagger} = -RT(\frac{\partial \ln k}{\partial p})$$

In this relationship, R and T represent the gas constant and temperature, respectively.

Similarly, the entropy of activation, $\Delta S^{\ddagger\circ}$, is a measure of entropy differences between the ground state and the transition state. Activation entropy is obtained by measuring the temperature dependence of rate constants according to the following relationship from transition state theory (117, 118, 120):

$$\ln\frac{k}{T} = \frac{-\Delta H^{\ddagger\circ}}{RT} + \frac{\Delta S^{\ddagger\circ}}{R} + \ln\frac{k_B\kappa}{h}$$

In this relationship, k_B represents the Boltzmann constant, κ is the transmission coefficient (usually assumed to be 1 in these experiments), and h is Planck's constant. Plotting ln (k/T) vs. (1/T) gives a line with slope $-\Delta H^{\ddagger}/R$ and intercept $\ln(k_B/h) + \Delta S^{\ddagger}/R$, allowing derivation of a value for the entropy of activation.

In principle, knowing how the volume or entropy of a reacting system changes between the ground state and transition state could provide information about transition state structure. For example, a loose transition state could have a greater volume and higher entropy than a tight transition state. By comparison with data for unimolecular and bimolecular reactions at carbon centers, observations of near-zero entropies and volumes of activation provided support in early work for expanded transition states for monoester reactions and tighter transition states for diester reactions (50, 121, 122). However, the measured values for volumes and entropies of activation include changes not just in the reacting system but also in the solvent (116, 117, 119, 123). For example, changes in polarity are typically observed in reaction transition states relative to ground states, and the solvent may accommodate these changes through reorganizations that can affect both volume and entropy of the system. Because the quantitative effects of these changes are not known, measures of activation volume and entropy should be considered with caution. Nevertheless, they provide empirical data about transition state properties that may someday be more directly correlated with transition state structure, so we include these data here.

Volumes of Activation for hydrolysis reactions

Reported volumes of activation are given in the below table. Phosphate ester hydrolysis reactions show negative activation volumes, which imply that the system contracts in volume in the

progression from ground state to transition state, consistent with concerted reactions where two species come together in the transition state. Monoester reactions show activation volumes close to zero, ranging from (0 to -5 cm^3/mol). In contrast, the single reported value for a phosphate diester hydrolysis reaction (-19 cm^3/mol) is considerably more negative, suggestive of a more compact transition state relative to the monoester reactions. These results are consistent with LFER and KIE evidence, which supports tighter transition state for diesters than for monoesters.

As shown in Table G1, activation volume has also been measured for a phosphorothioate hydrolysis reaction, providing an interesting comparison. As discussed in the respective sections of this supplement, phosphorothioate and phosphate monoester reactions show similar leaving group KIEs and LFERs, suggestive of similar large extents of leaving group dissociation in the transition state. The observation of stereochemical racemization for phosphorothioate reactions, consistent with formation of stable thiometaphosphate, provides further support for extensive leaving group bond cleavage in the transition state for phosphorothioate hydrolysis. The positive activation volume of +11 cm^3/mol observed for the phosphorothioate reaction suggests expansion of the system in the transition state relative to the phosphate ester, and is consistent with a loose and expanded transition state *en route* to free thiometaphosphate. These multiple experimental readouts strongly support extensive bond breaking to the leaving group in phosphorothioates, and the similar LFER and KIE results between phosphorothioate and phosphate monoesters provide additional strong support for the conclusion that phosphate monoesters proceed through loose transition states.

Most simply, the different activation volumes for phosphorothioate and phosphate monoesters are consistent with a looser transition state for the phosphorothioate. However, effects from desolvating the nucleophile and phosphoryl group for partial bonding in the phosphate ester transition state and differences that might arise from the different size, charge distribution, and polarizability of the sulfur atom can also impact these values. The effect of these differences on the volume *change* in the transition state is not obvious and would require further investigation.

Table G1. Volumes of activation reported in the literature.

	Compound	**Temp, °C**	**$\Delta V^{\ddagger}$, cm^3/mol**	**Ref.**
Phosphorothioate monoesters	2,4-dinitrophenyl thiophosphate dianion	25	**+11.0**	(124)
Monoester	Acetyl phosphate monoanion	39	**-0.6**	(125)
Monoester	Acetyl phosphate dianion	39	**-1.0**	(125)
Monoester	2,4-dinitrophenyl phosphate dianion	43	**-4.8**	(121)
Diester	Acetyl phenyl phosphate monoanion	60	**-19.0**	(125)

Entropies of Activation

Reported entropies of activation for reactions of phosphate esters are tabulated below. The values are separated by the identity of the nucleophile and sorted by $\Delta S^{\ddagger\circ}$ values. This arrangement makes evident a trend from monoesters to triesters, where increasing the number of substituents is associated with decreasing values of $\Delta S^{\ddagger\circ}$. As discussed above, activation parameters include changes in both solute and solvent, and so cannot uniquely identify transition states or mechanism. Nevertheless, the $\Delta S^{\ddagger\circ}$ values are consistent with the picture developed from LFER and KIE evidence, as triesters and diesters show larger reductions in entropies in the transition state, consistent with tighter association of nucleophile, phosphoryl group, and leaving group. The small and slightly positive values of $\Delta S^{\ddagger\circ}$ for monoesters are consistent with small changes or slight increases in entropy in the transition state, as would be expected if substantial cleavage of the bond to the leaving group is accompanied by little bond formation to the nucleophile.

Table G2. Entropies of activation for hydrolysis reactions

	Compound	**Ionic strength, M**	**$\Delta S^{\ddagger\circ}$, eu**	**Ref.**
Monoester	Acetyl phosphate dianion	6.6	**+8.4**	(126)
Monoester	Phenyl phosphate dianion	1	**+7.0**	(127)
Monoester	2,4-dinitrophenyl phosphate dianion	1	**+6.6**	(2)
Monoester	Acetyl phosphate dianion	0.6	**+3.7**	(50, 126)
Monoester	4-nitrophenyl phosphate dianion	1	**+3.5**	(1)
Monoester	Acetyl phosphate dianion	0.1	**+1.6**	(126)
Monoester	Acetyl phosphate dianion, 2nd order hydrolysis	6.6	**+1.1**	(126)
Monoester	ATP	0.5	**-3.0**	(45)
Diester	Bis-2,4-dinitrophenyl phosphate monoanion	1	**-25.5**	(4)
Diester	Acetyl phenyl phosphate monoanion	1	**-28.8**	(50)
Triester	2,4-dinitrophenyl 2-aryloxy-2-oxo-1,3,2-dioxaphosphorinan	1	**-35.6**	(55)

Table G3. Entropies of activation for attack by other oxygen nucleophiles

	Compound	**Ionic strength, M**	**$\Delta S^{\ddagger\circ}$, eu**	**Ref.**
Monoester	Acetyl phosphate dianion, 2nd order phosphorolysis reaction	5.8	**+12.0**	(126)
Triester	2,4-dinitrophenyl dibenzyl phosphate attack by formate	1	**-21.7**	(64)
Triester	2,4-dinitrophenyl dibenzyl phosphate attack by acetate	1	**-26.4**	(64)

Table G4. Entropies of activation for attack by amine nucleophiles

	Compound	**Ionic strength, M**	**$\Delta S^{\ddagger\circ}$, eu**	**Ref.**
Monoester	ATP, attack by imidazole	0.5	**-4**	(45)
Monoester	ATP, attack by pyridine	0.5	**-5**	(45)
Monoester	ATP, attack by 3-picoline	0.5	**-5**	(45)
Monoester	ATP, attack by 4-picoline	0.5	**-8**	(45)
Monoester	2,4-dinitrophenyl phosphate dianion, pyridine attack	1	**-19.4**	(44)
Diester	Bis-2,4-dinitrophenyl phosphate monoanion, pyridine attack	1	**-23.1**	(44)
Diester	Methyl 2,4-dinitrophenyl phosphate monoanion, pyridine attack	1	**-31.3**	(53)

H. Phosphoglucomutase: Supplemental Discussion

Recent x-ray crystallographic studies have challenged expectations from nonenzymatic reactions, reporting metaphosphate or phosphorane intermediates for some enzymes that catalyze phosphoryl transfer from monoesters (128-131). Metaphosphate would not be expected as an intermediate, as such an intermediate is not observed in solution and positioning of the nucleophile for addition would lessen the probability of forming such an intermediate (see (19) for additional discussion). These cases have not been further investigated, but we suspect that future studies will support alternative explanations such as an averaged electron density from equilibration of substrates and products within the crystal or the presence of entities other than metaphosphate giving rise to the observed electron density. Nevertheless, confirmation of bound metaphosphate would be of enormous importance, challenging and demanding revision of our current understanding.

The presence of a phosphorane intermediate would represent a still more radical departure from the solution reaction, moving the reaction pathway from proceeding through the bottom right corner of a two-dimensional reaction diagram (Figure 4C in the main text) to one proceeding through an intermediate in the top left corner. While the direction of this change is predicted from interactions with positively charged groups, as discussed above, such a drastic effect would be remarkable. Nevertheless, such an effect was proposed for the enzyme phosphoglucomutase, and the question of changes in enzymatic reaction coordinates is further discussed with the enzyme alkaline phosphatase in the next section (Section I).

Phosphoglucomutase catalyzes two phosphoryl transfer steps between the enzyme and glucose phosphate, a phosphate monoester. The phosphoryl group is transferred from one position on glucose to an Asp residue on the enzyme, and then returned to a different position on glucose. As discussed above, the expected reaction pathway for phosphoryl transfer from a monoester is a concerted reaction with a loose transition state (Figure H1A). In contrast, x-ray structural data for phosphoglucomutase from crystals grown in the presence of either of the substrates, glucose-1-phosphate or glucose-6-phosphate, suggested a surprising result: a stable pentacoordinate, trigonal bipyramidal intermediate bound to the Asp and glucose (Figure H1B) (128).

Because it was unexpected, this result was the subject of intense commentary and scrutiny (132-136). Soon after the pentacoordinate intermediate model was presented, it was noted that the observed electron density in the phosphoglucomutase structure might correspond not to a stable phosphorane but instead MgF_3^- (Figure H1C) (134), which had previously been reported to act as a transition state analog in phosphoryl transfer active sites (137) and would be difficult to distinguish from a central PO_3 by the diffraction approaches employed. Subsequent studies provided strong evidence in favor of bound MgF_3^- from ^{19}F and ^{31}P NMR and additional x-ray and NMR experiments that were used to evaluate the bound species under a variety of conditions (138, 139). In addition, results from kinetic studies and the observed inhibition of phosphoglucomutase by fluoride ions are consistent with the formation of a MgF_3^- transition state analog (138, 140). These results strongly suggest that a trigonal MgF_3^- species is bound in the phosphoglucomutase active site in a configuration nearly identical to that for the originally proposed phosphorane species (128), and further suggest that prior experiments reporting atomic

stoichiometry in the crystals as support for the phosphorane model (135, 141) lacked the precision necessary to provide a definitive resolution (139).

The phosphoglucomutase case illustrates general lessons. Structural studies have revolutionized enzymology, providing physical pictures of active site interactions and determining changes upon ligand binding and mutation. Transition state analogs for phosphoryl transfer including vanadate, AlF_4^-, and now MgF_3^-, have enabled the development of models of enzymatic transition state interactions (139, 142-147). Nevertheless, structural information does not, by itself, reveal mechanism or energetics and so must be combined with functional data. In assessing new structural results, consideration of the nonenzymatic reactions is a powerful tool for developing mechanistic models that can be further tested through kinetic studies, and for recognizing when such tests are particularly important. The phosphoglucomutase example provides a reminder of the synergy between kinetics, chemical mechanism, and structure in understanding enzymes and their catalysis.

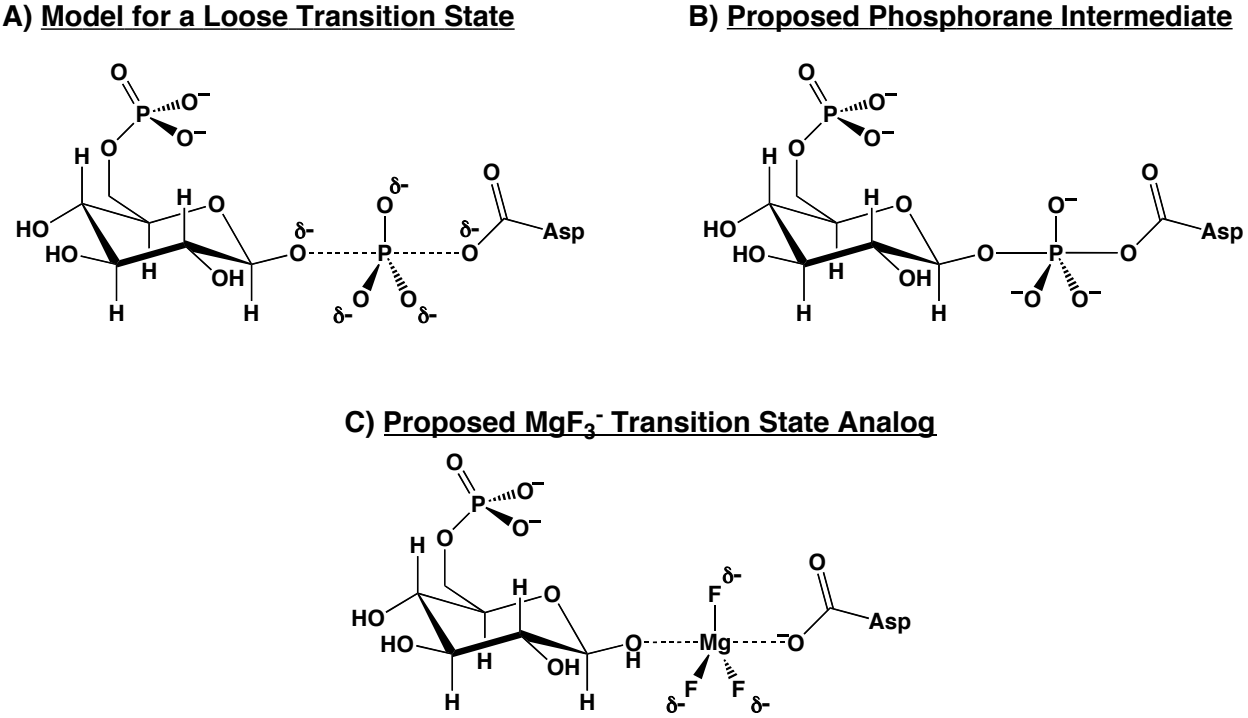

Figure H1. (A) The expected transition state for the phosphoglucomutase-catalyzed reaction is analogous to the loose transition state in the solution reaction. (B) The proposed phosphorane intermediate (128). This species would exist in a stable energy well bordered by two transition states and lower in energy than either phosphorylated species. When the phosphorane model was first proposed, it was noted that the axial P-O bond lengths were longer than observed in small-molecule alkylated phosphorane structures (128). (C) The alternative proposal of a bound MgF_3^- transition state analog complex (138, 139).

I. Alkaline Phosphatase: Supplemental Discussion

Alkaline phosphatase (AP) catalyzes the hydrolysis of a broad range of phosphate monoester substrates, and has been a paradigm for mechanistic studies of phosphoryl transfer and bimetallo hydrolase enzymes. Early work identified a covalent serine-phosphate intermediate and an active site with a bimetallo Zn^{2+}-center (148), and structural studies, including an x-ray structure with a vanadate transition state analog, have provided a model for transition state interactions in the AP active site (Figure I1) (149, 150).

Here we first focus on the question of the nature of the transition state for enzymatic phosphoryl transfer. AP has many positively charged functional groups in the active site (Figure I1) that can interact with the transferred phosphoryl group. Could this multitude of interactions result in a substantially rearranged energy landscape for AP-catalyzed phosphoryl transfer with a tighter transition state, even though, as discussed above, model studies with single metal ion interactions showed no significant perturbation (42, 151)?

Results from initial experiments using both thio-effects and LFERs were taken as evidence for such a change. AP-catalyzed phosphorothioate monoester hydrolysis is ~100-fold slower than phosphate monoester hydrolysis (69). As thio-substitution slows nonenzymatic reactions of phosphate triesters and speeds reactions of phosphate monoesters, this observation was taken to suggest an AP-catalyzed reaction via a tighter, triester-like reaction pathway. However, later experiments showed that thio-substitution disrupted catalytic interactions with the active site Arg residue (Figure I1, Arg166) (103). There are now several examples of thio-substitutions disrupting active site interactions (e.g., (152, 153)); in general thio-effects can provide incisive probes for active site interactions but do not report on the nature of enzymatic transition states.

Early LFER data were also cited to support a tighter transition state for AP-catalyzed reactions (154, 155). In general LFERs are problematic for enzymatic reactions because changes introduced to modulate the electronic properties of nucleophiles or leaving groups also introduce structural changes that can affect binding and orientation, and such effects can be difficult or impossible to deconvolute. But AP has evolved to accept a wide variety of leaving groups to provide phosphate required for growth, and structural studies indicate an open active site without identifiable interactions beyond the leaving group oxygen atom (149) Thus, AP would appear to be an ideal enzyme for LFER approaches, and small measured values of β_{LG} of ~ -0.2 seemed to provide evidence for a tight transition state with little bond cleavage to the leaving group (154, 155). However, other studies revealed that the rates of some AP-catalyzed reactions are limited by binding of substrates or release of bound product, rather than the chemical step, so that these LFERs provided no information about the chemical transition state ((100) and references therein).

These and other early studies set the stage for identifying substrates and conditions for which AP reactions could be carried out with the chemical step rate-limiting. LFERs for k_{cat}/K_M, the second-order reaction starting with free enzyme and substrate, were obtained with

phosphorothioate (70, 103) and alkyl phosphate substrates (100, 102), yielding large, negative values for β_{LG} of -0.8 and -0.85, respectively. These values are consistent with expectations for a loose, solution-like transition states once the nucleophile identity and effect from the Zn^{2+}-leaving group interaction are accounted for (100, 104). Subsequent KIE studies with AP reinforced these conclusions ((101); and see Supplemental Section F).

These studies were in turn foundational for incisive probes of the effects of cationic interactions on the AP transition state. Arg166 coordinates two nonbridging oxygen atoms in transition state models for AP (Figure I1). If these interactions lead to tightening of the transition state, as suggested in the literature, then a more negative β_{LG} value would be predicted upon removal of the Arg residue by mutation. In contrast to that prediction, a direct comparison of leaving group LFERs for alkyl phosphates for wild-type and Arg166Ser AP enzymes revealed no increase in steepness and nearly identical slopes, suggesting that arginine coordination does not significantly affect transition state character (102). In addition, measurement of individual reaction steps for these enzymes indicated that Arg coordination strengthens binding by about 3 kcal/mol and contributes an additional 1-2 kcal/mol of additional transition state stabilization (156). Thus, arginine coordination of the phosphoryl oxygen atoms can contribute to catalysis without tightening the transition state. This arginine residue may make preferential interactions with the oxygen of the transferred phosphoryl group in the transition state geometry, and may also help to position the transferred phosphoryl group with respect to the nucleophile and help position the leaving group for stabilization by an active site Zn^{2+} ion (152, 156-158).

Another incisive test of possible transition state effects of AP-active site interactions used the Arg166 mutant and focused on the Zn^{2+} bimetallo site and other remaining interactions. AP has what is referred to as 'promiscuous activity' for hydrolysis of sulfate esters, providing a low level of catalysis for this alternative reaction (8, 159). As the transferred sulfuryl group has one less negative charge than the transferred phosphoryl group, weaker electrostatic interactions would be expected with the sulfuryl group and thus less perturbation of the transition state. However, identical LFERs and leaving group KIEs are observed for phosphate and sulfate esters, both in solution and in AP-catalyzed reaction (104, 105). Thus, despite the preponderance of positive charge and multiple active site interactions, there is no indication of a perturbed transition state in AP-catalyzed reactions.

Overall, LFER and KIE studies support a transition state for AP-catalyzed reactions that is similar or identical to that for the corresponding solution reactions, although this is not proven. Similarly strong evidence for a loose enzymatic phosphoryl transfer transition state has been acquired for protein tyrosine phosphatases from LFER, KIE, and mutagenesis experiments (75, 106-109, 152, 157, 160-162).

How then does AP stabilize its transition state and achieve rate enhancements of well over 10^{20} fold? Large enzymatic rate enhancements seem to arise from multiple catalytic contributions (163, 164), and AP is no exception to this rule, apparently using each of the catalytic mechanisms outlined above. It is likely that an interaction of one of the active site Zn^{2+} ions stabilizes the leaving group, providing a large catalytic effect. Interaction of the serine nucleophile with the other Zn^{2+} ion likely helps to deprotonate the serine, providing a stronger nucleophile and a modest rate advantage. A large rate advantage may be provided by active site

interactions that position the serine and the reactive phosphoryl group with respect to one another through multiple electrostatic and hydrogen bonding interactions with the phosphoryl oxygen atoms. The interactions with the transferred phosphoryl group may provide additional catalysis if they are positioned to interact more strongly with the planar PO_3 geometry present in the transition state than with the tetrahedral ground state configuration, as has been suggested (152, 156-158, 165, 166).

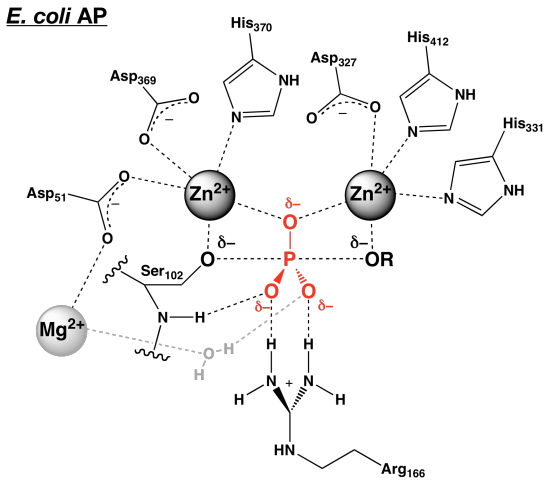

Figure I1. Schematic of the active site of *E. coli* AP and interactions with a transition state model (149, 150). The transferred phosphoryl group is shown in red.

J. Ras GTPase: Supplemental Discussion

Ras and related proteins have been studied extensively as paradigms for molecular switches that link enzymatic activity to cell regulatory signals through conformational change (167). Ras catalyzes the hydrolysis of GTP, yielding GDP and subsequently turning signaling off (Figure J1A). Ras proteins have low intrinsic levels of GTPase activity, with catalysis typically only about 10^5 fold faster than nonenzymatic hydrolysis (168), and their GTPase activity is enhanced by about five orders of magnitude upon binding to GTPase activating proteins (GAPs) (169, 170).

The catalytic mechanism of the intrinsic Ras GTPase became a topic of extensive discussion when structural studies did not find an obvious candidate for a general base in the active site (171-175). In the quest to find enzymatic interactions that could fulfill the role of a general base, a new mechanism, referred to as "substrate-assisted catalysis", was proposed in which the GTP substrate itself acted as the catalytic base, deprotonating the water nucleophile for hydroxide attack (176, 177) (Figure J1B). The mechanism was evaluated through experiments in which active site mutations were used to perturb the apparent pK_a of the terminal phosphate group of the enzyme-bound substrate, which was in turn measured by NMR and activity assays (178, 179). The relationship between reactivity and pK_a was plotted as a LFER, which showed a linear relationship for the series of mutants. The observed linear relationship supported the conclusion that the activities of the enzymes were linked to the pK_a of bound GTP. Nevertheless, LFERs are correlations, and a correlation such as this could arise from any of a number effects; it need not indicate that GTP functions as a general base in the reaction.

Indeed, several observations suggested that this relationship is more complicated, involving a pH-dependent conformational change. The change in the ^{31}P NMR spectrum was assigned to protonation of the γ-phosphoryl group, as noted above, but the observed chemical shifts for all three phosphoryl groups of GTP (α, β, & γ) changed; however, for free ATP only the γ-phosphoryl group changes chemical shift upon protonation of the γ-phosphoryl group (180). Further, in the ^{31}P NMR experiments used to measure the pK_a values, two peaks were observed for each phosphoryl group at pH values near the pK_a, suggestive of a process slower than expected for a simple protonation (178). Vibrational spectroscopy indicated that the protein partially denatures at pH values near the pK_a values measured for protein-bound GTP (181). These observations suggest that the observed correlations are related to a local conformational rearrangement that may or may not be coupled to protonation of the γ-phosphoryl group. Regardless, the measured pK_a is a complex readout of multiple changes and not simply a gauge of local electrostatics and the results therefore not provide support for a substrate-assisted catalysis mechanism (181).

Returning to the general base, is one even needed in the Ras reaction? As discussed in the main text, the low value for β_{NUC} for monoester reactions suggests that changing the pK_a of the water nucleophile by deprotonating it with a general base to form hydroxide is not expected to provide a large rate enhancement. As detailed above, the expected difference in rate constant between hydroxide and water attack on a monoester is small, and β_{NUC} follows a similar shallow slope for NTP hydrolysis, with $\beta_{NUC} = 0.1$ (42). Thus, based on the expected loose transition state from the solution reaction, a general base would not be needed for the Ras GTPase activity. Residues that

can act as general bases may help position attacking groups, in this case water, and also provide a route for the ultimate removal of a proton subsequent to the transition state for the reaction (182).

At the time that the substrate-assisted general base model was proposed, experiments had not been performed to directly evaluate transition state properties in the Ras-catalyzed GTPase reaction, although the simplest expectation would be that the enzyme did not change the transition state. Subsequent KIE studies have observed leaving group KIEs for the Ras-catalyzed reaction of ~1.02, as expected for a loose transition state that is similar to that observed for solution reactions (110, 111) (see also Section F).

Given the current working model of a loose transition state for Ras and other GTPases, how do these enzymes achieve their catalysis? X-ray structures have revealed a water molecule that appears to be situated for attack on the γ-phosphorus atom (183, 184) (Figure J1C). Thus, positioning may provide a significant fraction of the modest rate enhancement by Ras. Further, the residues surrounding this water molecule appear to become more ordered upon binding of GAP (183), so this effect could account for a significant fraction of the $\sim 10^5$ fold rate enhancement provided by GAP. The remainder of the GAP effect was predicted based on consideration of features of a loose transition state. Whereas catalysis from interactions with nonbridging phosphoryl oxygen atoms of the β-phosphoryl group of GTP and ATP are often discussed, interactions with the β-γ-bridge oxygen atoms were rarely invoked. However, this atom undergoes the largest change in charge in going from the ground state to the transition state, and thus is a prime candidate for the preferential transition state interactions that are required for catalysis. Because of this, it was proposed that an Arg residue from GAP would be inserted into a crevice in Ras and reach this oxygen atom (182). Subsequent x-ray structures have provided strong evidence for a so-called “arginine finger” that can interact with the leaving group oxygen atom and an oxygen of the γ-phosphoryl group in RasGAP and related enzymes (137, 170, 183, 185-187) (see also(188, 189)) (Figure J1C). Mutagenesis of this arginine reduces GAP activation by 10^2-10^3–fold (170, 190, 191), supporting a catalytic role for this interaction. The Ras-GAP GTPase example illustrates how understanding of nonenzymatic phosphoryl transfer reactions can inform and enrich investigations of important biological enzymes.

A. Hydrolysis of Mg-GTP

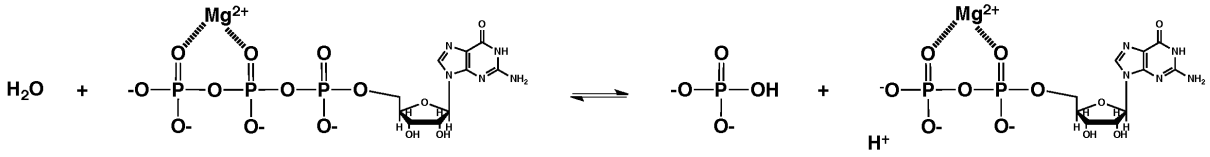

B. Proposed substrate-assisted catalysis mechanism

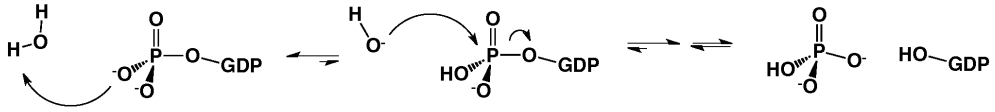

C. Arginine finger of GAP positioned near β-γ bridging oxygen

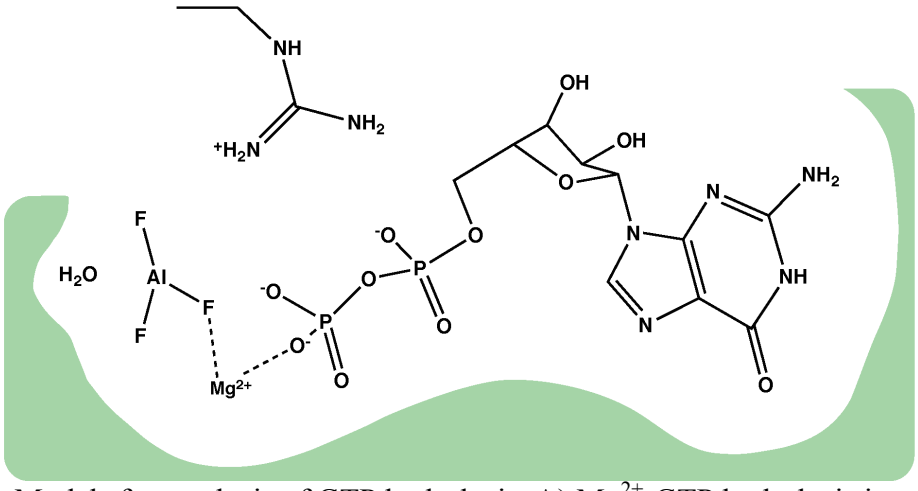

Figure J1. Models for catalysis of GTP hydrolysis. A) Mg^{2+}-GTP hydrolysis in solution. B) Proposed substrate-assisted catalysis mechanism. C) A schematic for the active site of Ras and related enzymes with GDP•AlF_3 bound in the active site. An arginine residue from GAP interacts with the GDP oxygen atom corresponding to the leaving group oxygen in GTP hydrolysis (137, 170, 183, 185-187).

K. References for Supplemental Material

1. Kirby AJ, Jencks WP. 1965. Reactivity of nucleophilic reagents toward p-nitrophenyl phosphate dianion. *J. Am. Chem. Soc.* 87: 3209-16
2. Kirby AJ, Varvoglis AG. 1967. Reactivity of phosphate esters. Monoester hydrolysis. *J. Am. Chem. Soc.* 89: 415-23
3. Lassila JK, Herschlag, D. 2008. Promiscuous sulfatase activity and thio-effects in a phosphodiesterase of the alkaline phosphatase superfamily. *Biochemistry* 47: 12853-59
4. Kirby AJ, Younas M. 1970. Reactivity of phosphate esters. Diester hydrolysis. *J. Chem. Soc. B*: 510-13
5. Chin J, Banaszczyk M, Jubian V, Zou X. 1989. Co(III) complex promoted hydrolysis of phosphate diesters: Comparison in reactivity of rigid cis-diaquotetraazacobalt(III) complexes. *J. Am. Chem. Soc.* 111: 186-90
6. Catrina I, Hengge AC. 1999. Comparisons of phosphorothioate and phosphate monoester transfer reactions: Activation parameters, solvent effects, and the effect of metal ions. *J. Am. Chem. Soc.* 121: 2156-63
7. Herschlag D, Piccirilli JA, Cech TR. 1991. Ribozyme-catalyzed and nonenzymatic reactions of phosphate diesters: Rate effects upon substitution of sulfur for a nonbridging phosphoryl oxygen atom. *Biochemistry* 30: 4844-54
8. O'Brien PJ, Herschlag D. 1998. Sulfatase activity of *E. coli* alkaline phosphatase demonstrates a functional link to arylsulfatases, an evolutionarily related enzyme family. *J. Am. Chem. Soc.* 120: 12369-70
9. Benkovic SJ, Benkovic PA. 1966. Studies on sulfate esters. I. Nucleophilic reactions of amines with p-nitrophenyl sulfate. *J. Am. Chem. Soc.* 88: 5504-11
10. Nikolic-Hughes I, O'Brien PJ, Herschlag D. 2005. Alkaline phosphatase catalysis is ultrasensitive to charge sequestered between the active site zinc ions. *J. Am. Chem. Soc.* 127: 9314-15
11. Friedman JM, Freeman S, Knowles JR. 1988. The quest for free metaphosphate in solution: Racemization at phosphorus in the transfer of the phospho group from aryl phosphate monoesters to tert-butyl alcohol in acetonitrile or in tert-butyl alcohol. *J. Am. Chem. Soc.* 110: 1268-75
12. Friedman JM, Knowles JR. 1985. The quest for free metaphosphate in solution--racemization at phosphorus in the transfer of the phospho group from phenyl phosphate to tert-butyl alcohol in acetonitrile. *J. Am. Chem. Soc.* 107: 6126-27
13. Cullis PM, Rous AJ. 1986. Stereochemical course of the phosphoryl transfer from adenosine 5'-diphosphate to alcohols in acetonitrile and the possible role of monomeric metaphosphate. *J. Am. Chem. Soc.* 108: 1298-300
14. Cullis PM, Rous AJ. 1985. Stereochemical course of phosphoryl transfer reactions of P1,P1-disubstituted pyrophosphate in aprotic solvent. A model for the enzyme-catalyzed "dissociative" phosphoryl tranfer. *J. Am. Chem. Soc.* 107: 6721-23
15. Cullis PM, Iagrossi A. 1986. Thiophosphoryl-transfer reactions: Stereochemical course of solvolysis of p-nitrophenyl thiophosphate in protic solvent and the possible role of thiometaphosphate. *J. Am. Chem. Soc.* 108: 7870-71
16. Cullis PM, Rajinder M, Wilkins DJ. 1987. Free monomeric thiometaphosphate in protic solvents: Complete racemization at phosphorus in the ethanolysis of 4-nitrophenyl thiophosphate. *J. Chem. Soc. Chem. Commun.* 1987: 1594-96

17. Halkides CJ, Frey PA. 1991. The mechanism of the hydrolysis of μ-monothiopyrophosphate. *J. Am. Chem. Soc.* 113: 9843-48
18. Lightcap ES, Frey PA. 1992. Discrete monomeric metaphosphate anion as an intermediate in the hydrolysis of μ-monothiopyrophosphate. *J. Am. Chem. Soc.* 114: 9750-55
19. Jencks WP. 1980. When is an intermediate not an intermediate? Enforced mechanisms of general acid-base catalyzed, carbocation, carbanion, and ligand-exchange reactions. *Acc. Chem. Res.* 13: 161-69
20. Gerratana B, Sowa GA, Cleland WW. 2000. Characterization of the transition-state structures and mechanisms for the isomerization and cleavage reactions of uridine 3 '-m-nitrobenzyl phosphate. *J. Am. Chem. Soc.* 122: 12615-21
21. Oivanen M, Schnell, R., Pfeiderer, W., Lonnberg, H. 1991. Interconversion and hydrolysis of monomethyl and monoisopropyl esters of adenosine 2'- and 3'-monophosphates: Kinetics and mechanisms. *J. Org. Chem.* 56: 3623-28
22. Jarvinen P, Oivanen, M., Lonnberg, H. 1991. Interconversion and phosphoester hydrolysis of 2',5'- and 3',5'-dinucleoside monophosphates: Kinetics and Mechanisms. *J. Org. Chem.* 56: 5396-401
23. Anslyn E, Breslow R. 1989. On the mechanism of catalysis by ribonuclease: Cleavage and isomerization of the dinucleotide UpU catalyzed by imidazole buffers. *J. Am. Chem. Soc.* 111: 4473-82
24. Lonnberg H, Stromberg R, Williams A. 2004. Compelling evidence for a stepwise mechanism of the alkaline cyclisation of uridine 3'-phosphate esters. 2: 2165-67
25. Humphry T, Forconi M, Williams NH, Hengge AC. 2002. An altered mechanism of hydrolysis for a metal-complexed phosphate diester. *J. Am. Chem. Soc.* 124: 14860-61
26. Rawlings J, Hengge AC, Cleland WW. 1997. Heavy-atom isotope effects on reactions of Co(III)-bound p-nitrophenyl phosphate: Nucleophilic displacements of p-nitrophenol and dissociation of p-nitrophenyl phosphate. *J. Am. Chem. Soc.* 119: 542-49
27. Taube H. 1952. Rates and mechanisms of substitution in inorganic complexes in solution. *Chem. Rev.* 50: 69-126
28. Hall CR, Inch TD. 1980. Phosphorus stereochemistry: Mechanistic implications of the observed stereochemistry of bond forming and breaking processes at phosphorus in some 5- and 6-membered cyclic phosphorus esters. *Tetrahedron* 36: 2059-95
29. Rowell R, Gorenstein DG. 1981. Multiple structure-reactivity correlations in the hydrolysis of epimeric 2-(aryloxy)-2-oxydioxaphosphorinanes. *J. Am. Chem. Soc.* 103: 5894-902
30. Gordillo B, Eliel EL. 1991. Use of 17O NMR in a stereochemical study of the alkaline hydrolysis of cyclic six-membered 2-aryl phosphates. *J. Am. Chem. Soc.* 113: 2172-77
31. Williams A. 1984. Effective charge and Leffler's index as mechanistic tools for reactions in solution. *Acc. Chem. Res.* 17: 425-30
32. Williams A. 2003. *Free energy relationships in organic and bio-organic chemistry*. Cambridge: The Royal Society of Chemistry
33. Bourne N, Williams A. 1984. Effective charge on oxygen in phosphoryl ($-PO_3^{2-}$) group transfer from an oxygen donor. *J. Org. Chem.* 49: 1200-04
34. Skoog MT, Jencks WP. 1984. Reactions of pyridines and primary amines with N-phosphorylated pyridines. *J. Am. Chem. Soc.* 106: 7597-606

35. Jencks WP, Haber MT, Herschlag D, Nazaretian KL. 1986. Decreasing reactivity with increasing nucleophile basicity. The effect of solvation on β_{nuc} for phosphoryl transfer to amines. *J. Am. Chem. Soc.* 108: 479-83
36. Ba-Saif SA, Waring MA, Williams A. 1991. Dependence of transition state structure on nucleophile in the reaction of aryl oxide anions with aryl diphenylphosphate esters. *J. Chem. Soc., Perkin Trans. 2*: 1653-59
37. Jencks WP. 1985. A primer for the Bema Hapothle. An empirical approach to the characterization of changing transition-state structures. *Chem. Rev.* 85: 511-27
38. Herschlag D, Jencks WP. 1989. Evidence that metaphosphate monoanion is not an intermediate in solvolysis reactions in aqueous solution. *J. Am. Chem. Soc.* 111: 7579-86
39. Hammond GS. 1955. A correlation of reaction rates. *J. Am. Chem. Soc.* 77: 334-38
40. Leffler JE. 1953. Parameters for the description of transition states. *Science* 117: 340-41
41. Jencks DA, Jencks WP. 1977. On the characterization of transition states by structure-reactivity coefficients. *J. Am. Chem. Soc.* 99: 7948-60
42. Admiraal SJ, Herschlag D. 1995. Mapping the transition state for ATP hydrolysis: implications for enzymatic catalysis. *Chem. Biol.* 2: 729-39
43. Herschlag D, Jencks WP. 1989. Phosphoryl transfer to anionic oxygen nucleophiles. Nature of the transition state and electrostatic repulsion. *J. Am. Chem. Soc.* 111: 7587-96
44. Kirby AJ, Varvoglis, A.G. 1968. The reactivity of phosphate esters: Reactions of monoesters with nucleophiles. Nucleophilicity independent of basicity in a bimolecular substitution reaction. *J. Chem. Soc. B*: 135-41
45. Admiraal SJ, Herschlag D. 1999. Catalysis of phosphoryl transfer from ATP by amine nucleophiles. *J. Am. Chem. Soc.* 121: 5837-45
46. Skoog MT, Jencks WP. 1983. Phosphoryl transfer between pyridines. *J. Am. Chem. Soc.* 105: 3356-57
47. Bourne N, Williams A. 1984. Evidence for a single transition state in the transfer of the phosphoryl group ($-PO_3^{2-}$) to nitrogen nucleophiles from pyridino-N-phosphonates. *J. Am. Chem. Soc.* 106: 7591-96
48. Bourne N, Williams, A. 1983. The question of concerted or stepwise mechanisms in phosphoryl group ($-PO_3^{2-}$) transfer to pyridines from isoquinoline-N-phosphonate. *J. Am. Chem. Soc.* 105: 3357-58
49. Jencks WP, Gilchrist, M. 1965. Reactions of nucleophilic reagents with phosphoramidate. *J. Am. Chem. Soc.* 87: 3199-209
50. Di Sabato GD, Jencks WP. 1961. Mechanism and catalysis of reactions of acyl phosphates. II. Hydrolysis. *J. Am. Chem. Soc.* 83: 4400-05
51. Lowry TH, Richardson KS. 1987. *Mechanism and Theory in Organic Chemistry*. New York: Harper Collins
52. Jameson GW, Lawlor, J.M. 1970. Aminolysis of N-phosphorylated pyridines. *J. Chem. Soc. B*: 53-57
53. Kirby AJ, Younas M. 1970. Reactivity of phosphate esters. Reactions of diesters with nucleophiles. *J. Chem. Soc. B*: 1165-72
54. Ye JD, Barth CD, Anjaneyulu PSR, Tuschl T, Piccirilli JA. 2007. Reactions of phosphate and phosphorothioate diesters with nucleophiles: comparison of transition state structures. *Org. Biomol. Chem.* 5: 2491-97
55. Khan SA, Kirby AJ. 1970. Reactivity of phosphate esters. Multiple structure-reactivity correlations for reactions of triesters with nucleophiles. *J. Chem. Soc. B*: 1172-82

56. Ba-Saif SA, Davis AM, Williams A. 1989. Effective charge distribution for attack of phenoxide ion on aryl methyl phosphate monoanion: studies related to the action of ribonuclease. *J. Org. Chem.* 54: 5483-86
57. Zalatan JG, Herschlag D. 2006. Alkaline phosphatase mono- and diesterase reactions: Comparative transition state analysis. *J. Am. Chem. Soc.* 128: 1293-303
58. Williams NH, Cheung W, Chin J. 1998. Reactivity of phosphate diesters doubly coordinated to a dinuclear cobalt(III) complex: Dependence of the reactivity on the basicity of the leaving group. *J. Am. Chem. Soc.* 120: 8079-87
59. Williams NH, Wyman P. 2001. Base catalysed phosphate diester hydrolysis. *Chem. Commun.*: 1268-69
60. Davis AM, Hall AD, Williams A. 1988. Charge Description of Base-Catalyzed Alcoholysis of Aryl Phosphodiesters - a Ribonuclease Model. *J. Am. Chem. Soc.* 110: 5105-08
61. Kosonen M, Youseti-Salakdeh E, Stromberg R, Lonnberg H. 1997. Mutual isomerization of uridine 2'- and 3'- alkylphosphates and cleavage to a 2',3'-cyclic phosphate: the effect of the alkyl group on the hydronium- and hydroxide-ion-catalyzed reactions. *J. Chem. Soc., Perkin Trans. 2* 1997: 2661-66
62. Satoh K, Inoue Y. 1972. Synthesis and reaction of a series of substituted benzyl esters of guanosine 3'-phosphate. *Chem. Lett.* 1972: 1097-100
63. Brown DM, Usher DA. 1965. Hydrolysis of hydroxyalkyl phosphate esters: effect of changing ester group. *J. Chem. Soc.* 1965: 6558-64
64. Gorenstein DG, Lee YG. 1977. Nucleophilic catalysis in the hydrolysis of 2,4-dinitrophenyl dibenzyl phosphate. *J. Am. Chem. Soc.* 99: 2258-63
65. Ba-Saif SA, Waring MA, Williams A. 1990. Single transition state in the transfer of a neutral phosphoryl group between phenoxide ion nucleophiles in aqueous-solution. *J. Am. Chem. Soc.* 112: 8115-20
66. Donarski WJ, Dumas DP, Heitmeyer DP, Lewis VE, Raushel FM. 1989. Structure-activity relationships in the hydrolysis of substrates by the phosphotriesterase from *Pseudomonas diminuta*. *Biochemistry* 28: 4650-55
67. Hong SB, Raushel FM. 1996. Metal-substrate interactions facilitate the catalytic activity of the bacterial phosphotriesterase. *Biochemistry* 35: 10904-12
68. Milstien S, Fife TH. 1967. Hydrolysis of S-aryl phosphorothioates. *J. Am. Chem. Soc.* 89: 5820-&
69. Breslow R, Katz I. 1968. Relative reactivities of p-nitrophenyl phosphate and phosphorothioate toward alkaline phosphatase and in aqueous hydrolysis. *J. Am. Chem. Soc.* 90: 7376-77
70. Hollfelder F, Herschlag D. 1995. The nature of the transition state for enzyme-catalyzed phosphoryl transfer. Hydrolysis of O-aryl phosphorothioates by alkaline phosphatase. *Biochemistry* 34: 12255-64
71. Burgers PMJ, Eckstein F. 1979. Diastereomers of 5'-O-Adenosyl 3'-O-Uridyl phosphorothioate: Chemical synthesis and enzymatic properties. *Biochemistry* 18: 592-96
72. Almer H, Stromberg R. 1996. Base catalysis and leaving group dependence in intramolecular alcoholysis of uridine 3'-(aryl phosphorothioate)s. *J. Am. Chem. Soc.* 118: 7921-28
73. Heath DF. 1956. The effects of substituents on the rates of hydrolysis of some organophosphorus compounds. Part II. Rates in neutral solutions. *J. Chem. Soc.*: 3804-09

74. Fanni T, Taira K, Gorenstein DG, Vaidyanathaswamy R, Verkade JG. 1986. Steroelectronic effects in the hydrolysis of bicyclic and acyclic phosphates and phosphorothioates. *J. Am. Chem. Soc.* 108: 6311-14
75. Hengge AC. 2002. Isotope effects in the study of phosphoryl and sulfuryl transfer reactions. *Acc. Chem. Res.* 35: 105-12
76. Gorenstein DG, Lee YG, Kar D. 1977. Kinetic isotope effects in reactions of aryl-O-18-2,4-dinitrophenyl dibenzyl phosphate and aryl-O-18-2,4-dinitrophenyl phosphate. Evidence for monomeric metaphosphate. *J. Am. Chem. Soc.* 99: 2264-67
77. Hengge AC, Cleland WW. 1990. Direct measurement of transition-state bond cleavage in hydrolysis of phosphate esters of p-nitrophenol. *J. Am. Chem. Soc.* 112: 7421-22
78. Hengge AC, Edens WA, Elsing H. 1994. Transition-state structures for phosphoryl-transfer reactions of p-nitrophenyl phosphate. *J. Am. Chem. Soc.* 116: 5045-49
79. Catrina IE, Hengge AC. 2003. Comparisons of phosphorothioate with phosphate transfer reactions for a monoester, diester, and triester: Isotope effect studies. *J. Am. Chem. Soc.* 125: 7546-52
80. Grzyska PK, Czyryca PG, Purcell J, Hengge AC. 2003. Transition state differences in hydrolysis reactions of alkyl versus aryl phosphate monoester monoanions. *J. Am. Chem. Soc.* 125: 13106-11
81. Grzyska PK, Czyryca PG, Purcell J, Hengge AC. 2007. Transition state differences in hydrolysis reactions of alkyl versus aryl phosphate monoester monoanions *J. Am. Chem. Soc.* 129: 5298
82. Czyryca PG, Hengge AC. 2001. The mechanism of the phosphoryl transfer catalyzed by *Yersinia* protein-tyrosine phosphatase: a computational and isotope effect study. *Biochim. Biophys. Acta.* 1547: 245-53
83. Hengge AC, Tobin AE, Cleland WW. 1995. Studies of transition-state structures in phosphoryl transfer reactions of phosphodiesters of p-nitrophenol. *J. Am. Chem. Soc.* 117: 5919-26
84. Hengge AC, Cleland WW. 1991. Phosphoryl-transfer reactions of phosphodiesters: Characterization of transition states by heavy-atom isotope effects. *J. Am. Chem. Soc.* 113: 5835-41
85. Cassano AG, Anderson VE, Harris ME. 2002. Evidence for direct attack by hydroxide in phosphodiester hydrolysis. *J. Am. Chem. Soc.* 124: 10964-65
86. Melander L, Saunders WH, Jr. 1980. *Reaction Rates of Isotopic Molecules*. New York: John Wiley & Sons, Inc.
87. Cassano AG, Anderson VE, Harris ME. 2004. Understanding the transition states of phosphodiester bond cleavage: Insights from heavy atom isotope effects. *Biopolymers* 73: 110-29
88. Caldwell SR, Raushel FM, Weiss PM, Cleland WW. 1991. Transition-state structures for enzymatic and alkaline phosphotriester hydrolysis. *Biochemistry* 30: 7444-50
89. Anderson MA, Shim H, Raushel FM, Cleland WW. 2001. Hydrolysis of phosphotriesters: Determination of transition states in parallel reactions by heavy-atom isotope effects. *J. Am. Chem. Soc.* 123: 9246-53
90. Hoff RH, Larsen P, Hengge AC. 2001. Isotope effects and medium effects on sulfuryl transfer reactions. *J. Am. Chem. Soc.* 123: 9338-44
91. Younker JM, Hengge, A.C. 2004. A mechanistic study of the alkaline hydrolysis of diaryl sulfate diesters. *J. Org. Chem.* 69: 9043-48

92. Hengge AC, Martin BL. 1997. Isotope effect studies on the calcineurin phosphoryl-transfer reaction: Transition state structure and effect of calmodulin and Mn^{2+}. *Biochemistry* 36: 10185-91
93. Martin BL, Jurado LA, Hengge AC. 1999. Comparison of the reaction progress of calcineurin with Mn^{2+} and Mg^{2+}. *Biochemistry* 38: 3386-92
94. Hoff RH, Mertz P, Rusnak F, Hengge AC. 1999. The transition state of the phosphoryl-transfer reaction catalyzed by the lambda Ser/Thr protein phosphatase. *J. Am. Chem. Soc.* 121: 6382-90
95. McWhirter C, Lund EA, Tanifum EA, Feng G, Sheikh QI, et al. 2008. Mechanistic study of protein phosphatase-1 (PP1), a catalytically promiscuous enzyme. *J. Am. Chem. Soc.* 130: 13673-82
96. Jones JP, Weiss PM, Cleland WW. 1991. Secondary ^{18}O isotope effects for hexokinase-catalyzed phosphoryl transfer from ATP. *Biochemistry* 30: 3634-39
97. Gerratana B, Frey PA, Cleland WW. 2001. Characterization of the transition-state structure of the reaction of kanamycin nucleotidyltransferase by heavy-atom kinetic isotope effects. *Biochemistry* 40: 2972-77
98. Sowa GA, Hengge AC, Cleland WW. 1997. 18O isotope effects support a concerted mechanism for ribonuclease A. *J. Am. Chem. Soc.* 119: 2319-20
99. Cassano AG, Anderson VE, Harris ME. 2004. Analysis of solvent nucleophile isotope effects: Evidence for concerted mechanisms and nucleophilic activation by metal coordination in nonenzymatic and ribozyme-catalyzed phosphodiester hydrolysis. *Biochemistry* 43: 10547-59
100. O'Brien PJ, Herschlag D. 2002. Alkaline phosphatase revisited: Hydrolysis of alkyl phosphates. *Biochemistry* 41: 3207-25
101. Zalatan JG, Catrina I, Mitchell R, Grzyska PK, O'Brien PJ, et al. 2007. Kinetic isotope effects for alkaline phosphatase reactions: Implications for the role of active-site metal ions in catalysis. *J. Am. Chem. Soc.* 129: 9789-98
102. O'Brien PJ, Herschlag D. 1999. Does the active site arginine change the nature of the transition state for alkaline phosphatase-catalyzed phosphoryl transfer? *J. Am. Chem. Soc.* 121: 11022-23
103. Holtz KM, Catrina IE, Hengge AC, Kantrowitz ER. 2000. Mutation of Arg-166 of alkaline phosphatase alters the thio effect but not the transition state for phosphoryl transfer. Implications for the interpretation of thio effects in reactions of phosphatases. *Biochemistry* 39: 9451-58
104. Nikolic-Hughes I, Rees DC, Herschlag D. 2004. Do electrostatic interactions with positively charged active site groups tighten the transition state for enzymatic phosphoryl transfer? *J. Am. Chem. Soc.* 126: 11814-19
105. Catrina I, O'Brien PJ, Purcell J, Nikolic-Hughes I, Zalatan JG, et al. 2007. Probing the origin of the compromised catalysis of *E. coli* alkaline phosphatase in its promiscuous sulfatase reaction. *J. Am. Chem. Soc.* 129: 5760-65
106. McCain DF, Catrina IE, Hengge AC, Zhang ZY. 2002. The catalytic mechanism of Cdc25A phosphatase. *J. Biol. Chem.* 277: 11190-200
107. McCain DF, Grzyska PK, Wu L, Hengge AC, Zhang ZY. 2004. Mechanistic studies of protein tyrosine phosphatases YopH and Cdc25A with m-nitrobenzyl phosphate. *Biochemistry* 43: 8256-64

108. Grzyska PK, Kim Y, Jackson MD, Hengge AC, Denu JM. 2004. Probing the transition-state structure of dual-specificity protein phosphatases using a physiological substrate mimic. *Biochemistry* 43: 8807-14
109. Hengge AC, Sowa GA, Wu L, Zhang ZY. 1995. Nature of the transition state of the protein-tyrosine phosphatase-catalyzed reaction. *Biochemistry* 34: 13982-87
110. Du XL, Black GE, Lecchi P, Abramson FP, Sprang SR. 2004. Kinetic isotope effects in Ras-catalyzed GTP hydrolysis: Evidence for a loose transition state. *Proc. Natl. Acad. Sci. U.S.A.* 101: 8858-63
111. Du XL, Sprang SR. 2009. Transition state structures and the roles of catalytic residues in GAP-facilitated GTPase of Ras as elucidated by ^{18}O kinetic isotope effects. *Biochemistry* 48: 4538-47
112. Whalley E. 1967. High pressure. *Annu. Rev. Phys. Chem.* 18: 205-32
113. Whalley E. 1959. Pressure effect and mechanism in acid catalysis. *Trans. Faraday Soc.* 55: 798-808
114. Blandamer MJ, Burgess J, Engberts JBFN. 1985. Activation parameters for chemical reactions in solution. *Chem. Soc. Rev.* 14: 237-64
115. Hamann SD. 1964. High pressure chemistry. *Annu. Rev. Phys. Chem.* 15: 349-70
116. le Noble WJ, Kelm H. 1980. Chemistry in compressed solutions. *Angew. Chem. Int. Ed. Engl.* 19: 841-946
117. Evans MG, Polanyi M. 1935. Some applications of the transition state method to the calculation of reaction velocities, especially in solution. *Trans. Faraday Soc.* 31: 875-94
118. Blandamer MJ, Burgess J, Robertson RE, Scott JMW. 1982. Dependence of equilibrium and rate constants on temperature and pressure. *Chem. Rev.* 82: 259-86
119. Van Eldik R, Asano T, le Noble WJ. 1989. Activation and reaction volumes in solution. 2. *Chem. Rev.* 89: 549-688
120. Eyring H. 1935. The activated complex in chemical reactions. *J. Chem. Phys.* 3: 107-15
121. Ramirez F, Marecek J, Minore J, Srivastava S, le Noble W. 1986. On the freeness of the metaphosphate anion in aqueous solution. *J. Am. Chem. Soc.* 108: 348-49
122. Long FA, Pritchard JG, Stafford FE. 1957. Entropies of activation and mechanism for the acid-catalyzed hydrolysis of ethylene oxide and its derivatives. *J. Am. Chem. Soc.* 79: 2362-64
123. Drljaca A, Hubbard, C.D., van Eldik, R., Asano, T., Basilevsky, M.V., le Noble, W.J. 1998. Activation and reaction volumes in solution. 3. *Chem. Rev.* 98: 2167-289
124. Burgess J, Blundell N, Cullis PM, Hubbard CD, Misra R. 1988. Evidence for free monomeric thiometaphosphate anion in aqueous solution. *J. Am. Chem. Soc.* 110: 7900-01
125. Di Sabato G, Jencks WP, Whalley E. 1962. The effect of pressure on the spontaneous hydrolysis of acetyl phosphate mono-anion and di-anion and of acetyl phenyl phosphate mono-anion. *Can. J. Chem.* 40: 1220-24
126. Herschlag D, Jencks WP. 1986. Pyrophosphate formation from acetyl phosphate and ortho-phosphate anions in concentrated aqueous salt-solutions does not provide evidence for a meta-phosphate intermediate. *J. Am. Chem. Soc.* 108: 7938-46
127. Lad C, Williams NH, Wolfenden R. 2003. The rate of hydrolysis of phosphomonoester dianions and the exceptional catalytic proficiencies of protein and inositol phosphatases. *Proc. Natl. Acad. Sci. U.S.A.* 100: 5607-10

128. Lahiri SD, Zhang GF, Dunaway-Mariano D, Allen KN. 2003. The pentacovalent phosphorus intermediate of a phosphoryl transfer reaction. *Science* 299: 2067-71
129. Choe JY, Iancu CV, Fromm HJ, Honzatko RB. 2003. Metaphosphate in the active site of fructose-1,6-bisphosphatase. *J. Biol. Chem.* 278: 16015-20
130. Leiros I, McSweeney S, Hough E. 2004. The reaction mechanism of phospholipase D from Streptomyces sp strain PMF. Snapshots along the reaction pathway reveal a pentacoordinate reaction intermediate and an unexpected final product. *J. Mol. Biol.* 339: 805-20
131. de Macedo-Ribeiro S, Renirie R, Wever R, Messerschmidt A. 2008. Crystal structure of a trapped phosphate intermediate in vanadium apochloroperoxidase catalyzing a dephosphorylation reaction. *Biochemistry* 47: 929-34
132. Knowles JR. 2003. Seeing is believing. *Science* 299: 2002-03
133. Yarnell A. 2003. Identity of mystery atoms disputed. *Chem. Eng. News* 81: 30-31
134. Blackburn GM, Williams NH, Gamblin SJ, Smerdon SJ. 2003. Comment on "The pentacovalent phosphorus intermediate of a phosphoryl transfer reaction". *Science* 301: 1184c
135. Allen KN, Dunaway-Mariano D. 2003. Response to comment on "The pentacovalent phosphorus intermediate of a phosphoryl transfer reaction". *Science* 301: 1184d
136. Webster CE. 2004. High-energy intermediate or stable transition state analogue: Theoretical perspective of the active site and mechanism of beta-phosphoglucomutase. *J. Am. Chem. Soc.* 126: 6840-41
137. Graham DL, Lowe PN, Grime GW, Marsh M, Rittinger K, et al. 2002. MgF_3^- as a transition state analog of phosphoryl transfer. *Chem. Biol.* 9: 375-81
138. Baxter NJ, Olguin LF, Golicnik M, Feng G, Hounslow AM, et al. 2006. A Trojan horse transition state analogue generated by MgF_3^- formation in an enzyme active site. *Proc. Natl. Acad. Sci. U.S.A.* 103: 14732-37
139. Baxter NJ, Bowler MW, Alizadeh T, Cliff MJ, Hounslow AM, et al. 2010. Atomic details of near-transition state conformers for enzyme phosphoryl transfer revealed by MgF_3^- rather than by phosphoranes. *Proc. Natl. Acad. Sci. U.S.A.* 107: 4555-60
140. Golicnik M, Olguin LF, Feng G, Baxter NJ, Waltho JP, et al. 2009. Kinetic analysis of β-phosphoglucomutase and its inhibition by magnesium fluoride. *J. Am. Chem. Soc.* 131: 1575-88
141. Tremblay LW, Zhang G, Dai J, Dunaway-Mariano D, Allen KN. 2005. Chemical confirmation of a pentavalent phosphorane in complex with beta-phosphoglucomutase. *J. Am. Chem. Soc.* 127: 5298-99
142. Davies DR, Hol WGJ. 2004. The power of vanadate in crystallographic investigations of phosphoryl transfer enzymes. *FEBS Lett.* 577: 315-21
143. Chabre M. 1990. Aluminofluoride and beryllofluoride complexes: new phosphate analogs in enzymoloyg. *Trends. Biochem. Sci.* 15: 6-10
144. Wittinghofer A. 1997. Signaling mechanistics: Aluminum fluoride for molecule of the year. *Curr. Biol.* 7: R682-R85
145. Messmore JM, Raines RT. 2000. Pentavalent organo-vanadates as transition state analogues for phosphoryl transfer reactions. *J. Am. Chem. Soc.* 122: 9911-16
146. Deng H, Callender R, Huang Z, Zhang ZY. 2002. Is the PTPase-vanadate complex a true transition state analogue? *Biochemistry* 41: 5865-72

147. Baxter NJ, Blackburn GM, Marston JP, Hounslow AM, Cliff MJ, et al. 2008. Anionic charge is prioritized over geometry in aluminum and magnesium fluroide transition state analogs of phoshporyl transfer enzymes. *J. Am. Chem. Soc.* 130: 3952-58
148. Coleman JE. 1992. Structure and mechanism of alkaline phosphatase. *Annu. Rev. Biophys. Biomol. Struct.* 21: 441-83
149. Kim EE, Wyckoff HW. 1991. Reaction mechanism of alkaline phosphatase based on crystal structures. Two-metal ion catalysis. *J. Mol. Biol.* 218: 449-64
150. Holtz KM, Stec B, Kantrowitz ER. 1999. A model of the transition state in the alkaline phosphatase reaction. *J. Biol. Chem.* 274: 8351-54
151. Herschlag D, Jencks WP. 1987. The effect of divalent metal ions on the rate and transition-state structure of phosphoryl-transfer reactions. *J. Am. Chem. Soc.* 109: 4665-74
152. Zhang YL, Hollfelder F, Gordon SJ, Chen L, Keng YF, et al. 1999. Impaired transition state complementarity in the hydrolysis of O-arylphosphorothioates by protein-tyrosine phosphatases. *Biochemistry* 38: 12111-23
153. Brautigam CA, Steitz TA. 1998. Structural principles for the inhibition of the 3 '-5 ' exonuclease activity of *Escherichia coli* DNA polymerase I by phosphorothioates. *J. Mol. Biol.* 277: 363-77
154. Hall AD, Williams A. 1986. Leaving group dependence in the phosphorylation of *Escherichia coli* alkaline phosphatase by monophosphate esters. *Biochemistry* 25: 4784-90
155. Han R, Coleman JE. 1995. Dependence of the phosphorylation of alkaline phosphatase by phosphate monoesters on the pK_a of the leaving group. *Biochemistry* 34: 4238-45
156. O'Brien PJ, Lassila JK, Fenn TD, Zalatan JG, Herschlag D. 2008. Arginine coordination in enzymatic phosphoryl transfer: Evaluation of the effect of Arg166 mutations in *Escherichia coli* alkaline phosphatase. *Biochemistry* 47: 7663-72
157. Hoff RH, Wu L, Zhou B, Zhang ZY, Hengge AC. 1999. Does positive charge at the active sites of phosphatases cause a change in mechanism? The effect of the conserved arginine on the transition state for phosphoryl transfer in the protein-tyrosine phosphatase from *Yersinia*. *J. Am. Chem. Soc.* 121: 9514-21
158. Alhambra C, Wu L, Zhang ZY, Gao JL. 1998. Walden-inversion-enforced transition-state stabilization in a protein tyrosine phosphatase. *J. Am. Chem. Soc.* 120: 3858-66
159. O'Brien PJ, Herschlag D. 1999. Catalytic promiscuity and the evolution of new enzymatic activities. *Chem. Biol.* 6: R91-R105
160. Hengge AC, Denu JM, Dixon JE. 1996. Transition state structures for the native dual-specific phosphatase VHR and D92N and S131A mutants. Contributions to the driving force for catalysis. *Biochemistry* 35: 7084-92
161. Zhao Y, Zhang ZY. 1996. Reactivity of alcohols toward the phosphoenzyme intermediate in the protein tyrosine phosphatase-catalyzed reaction: Probing the transition state of the dephosphorylation step. *Biochemistry* 35: 11797-804
162. Hengge AC, Zhao Y, Wu L, Zhang ZY. 1997. Examination of the transition state of the low-molecular mass small tyrosine phosphatase 1. Comparisons with other protein phosphatases. *Biochemistry* 36: 7928-36
163. Kraut DA, Carroll KS, Herschlag D. 2003. Challenges in enzyme mechanism and energetics. *Annu. Rev. Biochem.* 72: 517-71

164. Jencks WP. 1987. *Catalysis in Chemistry and Enzymology*. New York: Dover Publications, Inc.
165. Zhang ZY, Wang Y, Wu L, Faumann EB, Stuckey JA, et al. 1994. The $Cys(X)_5Arg$ catalytic motif in phosphoester hydrolysis. *Biochemistry* 33: 15266-70
166. Zhang M, Zhou M, VanEtten RL, Stauffacher CV. 1997. Crystal structure of bovine low molecular weight phosphotyrosyl phosphatase complexed with the transition state analog vanadate. *Biochemistry* 36: 15-23
167. Bos JL, Rehmann H, Wittinghofer A. 2007. GEFs and GAPs: Critical elements in the control of small G proteins. *Cell* 129: 865-77
168. Mildvan AS. 1997. Mechanisms of signaling and related enzymes. *Proteins* 29: 401-16
169. Gideon P, John J, Frech M, Lautwein A, Clark R, et al. 1992. Mutational and kinetic analyses of the GTPase-activating protein (GAP)-p21 interaction: the C-terminal domain of GAP is not sufficient for full activity. *Mol. Cell. Biol.* 12: 2050-56
170. Ahmadian MR, Stege P, Scheffzek K, Wittinghofer A. 1997. Confirmation of the arginine-finger hypothesis for the GAP-stimulated GTP-hydrolysis reaction of Ras. *Nat. Struct. Biol.* 4: 686-89
171. DeVos AM, Tong L, Milburn MV, Matias PM, Jancarik J, et al. 1988. Three-dimensional structure of an oncogene protein: catalytic domain of human c-H-ras p21. *Science* 239: 888-93
172. Krengel U, Schlichting I, Scherer A, Schumann R, Frech M, et al. 1990. Three-dimensional structures of H-ras p21 mutants: molecular basis for their inability to function as signal switch peptides. *Cell* 62: 539-48
173. Milburn MV, Tong L, DeVos AM, Brunger A, Yamaizumi Z, et al. 1990. Molecular switch for signal transduction: structural differences between active and inactive forms of protooncogenic ras proteins. *Science* 247: 939-45
174. Pai EF, Krengel U, Petsko GA, Goody RS, Kabsch W, Wittinghofer A. 1990. Refined crystal structure of the triphosphate conformation of H-ras p21 at 1.35 Å resolution: implications for the mechanism of GTP hydrolysis. *EMBO J.* 9: 2351-59
175. Pai EF, Kabsch W, Krengel U, Holmes KC, John J, Wittinghofer A. 1989. Structure of the guanine nucleotide binding domain of the Ha-ras oncogene product p21 in the triphosphate conformation. *Nature* 341: 209-14
176. Langen R, Schweins T, Warshel A. 1992. On the mechanism of guanosine triphosphate hydrolysis in ras p21 proteins. *Biochemistry* 31: 8691-96
177. Schweins T, Langen R, Warshel A. 1994. Why have mutagenesis studies not located the general base in ras p21. *Nat. Struct. Biol.* 1: 476-84
178. Schweins T, Geyer M, Scheffzek K, Warshel A, Kalbitzer HR, Wittinghofer A. 1995. Substrate-assisted catalysis as a mechanism for GTP hydrolysis of p21ras and other GTP-binding proteins. *Nat. Struct. Mol. Biol.* 2: 36-44
179. Schweins T, Geyer M, Kalbitzer HR, Wittinghofer A, Warshel A. 1996. Linear free energy relationships in the intrinsic and GTPase activating protein stimulated guanosine 5'-triphosphate hydrolysis of p21ras. *Biochemistry* 35: 14225-31
180. Cohn M, Hughes TR. 1960. Phosphorus magnetic resonance spectra of adenosine diphosphate and triphosphate. Effect of pH. *J. Biol. Chem.* 235: 3250-53
181. Cheng H, Sukal S, Callender R, Leyh TS. 2001. γ-phosphate protonation and pH-dependent unfolding of the $Ras.GTP.Mg^{2+}$ complex: a vibrational spectroscopy study. *J. Biol. Chem.* 276: 9931-5

182. Maegley KA, Admiraal SJ, Herschlag D. 1996. Ras-catalyzed hydrolysis of GTP: A new perspective from model studies. *Proc. Natl. Acad. Sci. U.S.A.* 93: 8160-66
183. Scheffzek K, Ahmadian MR, Kabsch W, Wiesmuller L, Lautwein A, et al. 1997. The Ras-RasGAP complex: Structural basis for GTPase activation and its loss in oncogenic Ras mutants. *Science* 277: 333-38
184. Sprang SR. 1997. G protein mechanisms: Insights from structural analysis. *Annu. Rev. Biochem.* 66: 639-78
185. Rittinger K, Walker PA, Eccleston JF, Smerdon SJ, Gamblin SJ. 1997. Structure at 1.65 Å of RhoA and its GTPase-activating protein in complex with a transition-state analogue. *Nature* 389: 758-62
186. Pan X, Eathiraj S, Munson M, Lambright DG. 2006. TBC-domain GAPs for Rab GTPases accelerate GTP hydrolysis by a dual-finger mechanism. *Nature* 442: 303-06
187. Noel JP, Hamm HE, Sigler PB. 1993. The 2.2 Å crystal structure of transducin-alpha complexed with GTPγS. *Nature* 366: 654-63
188. Scrima A, Thomas C, Deaconescu D, Wittinghofer A. 2008. The Rap-RapGAP complex: GTP hydrolysis without catalytic glutamine and arginine residues. *EMBO J.* 27: 1145-53
189. Seewald MJ, Korner C, Wittinghofer A, Vetter IR. 2002. RanGAP mediates GTP hydrolysis without an arginine finger. *Nature* 415: 662-66
190. Albert S, Will E, Gallwitz D. 1999. Identification of the catalytic domains and their functionally critical arginine residues of two yeast GTPase-activating proteins specific for Ypt/Rab transport GTPases. *EMBO J.* 18: 5216-25
191. Graham DL, Eccleston JF, Lowe PN. 1999. The conserved arginine in Rho-GTPase-activating protein is essential for efficient catalysis but not for complex formation with Rho•GDP and aluminum fluoride. *Biochemistry* 38: 985-91